Cellular and Molecular Life Sciences (2023) 80:15
https://doi.org/10.1007/s00018-022-04664-w

ORIGINAL ARTICLE

CX3CR1 deficiency leads to impairment of immune surveillance in the epididymis

F. Barrachina[1,2] · K. Ottino[1,2] · L. J. Tu[1,2] · R. J. Soberman[2] · D. Brown[1,2] · S. Breton[3] · M. A. Battistone[1,2]

Received: 16 August 2022 / Revised: 9 November 2022 / Accepted: 9 December 2022 / Published online: 23 December 2022

Abstract

Mononuclear phagocytes (MPs) play an active role in the immunological homeostasis of the urogenital tract. In the epididymis, a finely tuned balance between tolerance to antigenic sperm and immune activation is required to maintain epididymal function while protecting sperm against pathogens and stressors. We previously characterized a subset of resident MPs that express the CX3CR1 receptor, emphasizing their role in antigen sampling and processing during sperm maturation and storage in the murine epididymis. Bacteria-associated epididymitis is the most common cause of intrascrotal inflammation and frequently leads to reproductive complications. Here, we examined whether the lack of functional CX3CR1 in homozygous mice ($CX3CR1^{EGFP/EGFP}$, KO) alters the ability of MPs to initiate immune responses during epididymitis induced by LPS intravasal–epididymal injection. Confocal microscopy revealed that CX3CR1-deficient MPs located in the initial segments of the epididymis displayed fewer luminal-reaching membrane projections and impaired antigen capture activity. Moreover, flow cytometry showed a reduction of epididymal KO MPs with a monocytic phenotype under physiological conditions. In contrast, flow cytometry revealed an increase in the abundance of MPs with a monocytic signature in the distal epididymal segments after an LPS challenge. This was accompanied by the accumulation of $CD103^+$ cells in the interstitium, and the prevention or attenuation of epithelial damage in the KO epididymis during epididymitis. Additionally, CX3CR1 deletion induced downregulation of *Gja1* (connexin 43) expression in KO MPs. Together, our study provides evidence that MPs are gatekeepers of the immunological blood-epididymis barrier and reveal the role of the CX3CR1 receptor in epididymal mucosal homeostasis by inducing MP luminal protrusions and by regulating the monocyte population in the epididymis at steady state as well as upon infection. We also uncover the interaction between MPs and $CD103^+$ dendritic cells, presumably through connexin 43, that enhance immune responses during epididymitis. Our study may lead to new diagnostics and therapies for male infertility and epididymitis by identifying immune mechanisms in the epididymis.

Keywords Mononuclear phagocytes · Immune regulation · Male infertility · Male reproductive tract · Mucosal immunology

Introduction

Mononuclear phagocytes (MPs) represent a heterogeneous cell population with distinct morphology, phenotype, and function in different organs [1–8]. These myeloid cells are involved in the maintenance of tissue homeostasis, inflammation, and activation of immune responses against infections [6–8]. MP subsets, including dendritic cells (DCs), monocytes, and macrophages, reside in peripheral tissues, such as the epididymis, and are all essential components of the immune system that connects innate and adaptive immunity [1–3, 7–12].

The epididymal mucosa is a particularly dynamic environment in which the interaction between spermatozoa, epithelial cells, and immunocytes is tightly regulated to

✉ M. A. Battistone
mbattistone@mgh.harvard.edu

1 Program in Membrane Biology, Department of Medicine, Massachusetts General Hospital and Harvard Medical School, Charlestown, MA, USA

2 Nephrology Division, Department of Medicine, Massachusetts General Hospital and Harvard Medical School, Charlestown, MA, USA

3 Centre Hospitalier Universitaire de Québec-Research Center, Department of Obstetrics, Gynecology, and Reproduction, Faculty of Medicine, Université Laval, Québec, QC, Canada

maintain homeostasis and distinguish self-cells from stressors [1–3, 13–15]. For instance, we have previously shown that epididymal epithelial clear cells (CCs) interact closely with MPs to mount an innate immune defense against bacterial antigens by rapidly upregulating pro-inflammatory mediators, such as *Cxcl10, Cxcl1, Cxcl2, Ccl5* and *Il6* [14]. Moreover, it has been reported that injection of lipopolysaccharide (LPS) from *Escherichia coli* into the vas deferens and distal epididymis increases the level of pro-inflammatory factors such as *Il6*, *Tnfa*, and *Il1b*, in the rat and mouse epididymal cauda [15, 16]. These molecules play key roles in immune cell recruitment to the epididymis upon infection.

A significant portion of male infertility is caused by infection, inflammation, and autoimmunity of the male reproductive tract [17–28]. However, many male infertility cases are still labeled idiopathic, illustrating our poor understanding of male reproductive physiology. Epididymitis is one of the most prevalent reasons for intrascrotal inflammation and often leads to reproductive complications [23–30]. Despite the deleterious effects of epididymitis on fertility and patient well-being, many subjects receive inadequate diagnostic, and therapeutic interventions [23, 29–31]. Thus, understanding how the epididymis mounts immune defense responses is of high clinical relevance. *Escherichia coli* infection is the most frequent etiology of epididymitis, which causes irreversible epididymal ductal obstruction and fibrotic tissue remodeling, and ultimately induces infertility [17, 18, 23–27, 32]. Bacterial antigen-induced epididymitis is characterized by a tremendous infiltration of neutrophils, monocytes, and macrophages into this organ [3, 14, 33]. These phagocytic cells are important first defenders upon infection and contribute to substantial tissue injury by releasing pro-inflammatory mediators that amplify the immune reaction [1, 3, 33–35].

Intraepithelial and interstitial MPs that express the CX3CR1 chemokine receptor are strategically positioned to maintain epididymal tissue homeostasis [1, 2, 4, 5, 13]. We have previously identified distinct functional and transcriptomic MP signatures in different epididymal regions (initial segments (IS), caput/corpus, and cauda) under physiological conditions [1, 2]. Interestingly, $CX3CR1^{+}$ MPs present unique morphological characteristics in the epididymis: intraepithelial MPs from the IS send numerous luminal reaching projections between epithelial cells, but this unique morphometrical characteristic was not observed in the more distal regions (corpus and cauda), where intraepithelial MPs mainly cover the base of the epithelium [1, 2, 4, 5, 13, 36]. In addition, we showed that MPs can partake in the capture and presentation of circulating antigens in the different segments of the epididymis [1, 2]. However, the molecular machinery that MPs employ to protect sperm from the immune system while ensuring immune activation against pathogens remains poorly characterized. In the current study, we examined whether the lack of functional CX3CR1 in homozygous ($CX3CR1^{EGFP/EGFP}$, KO) mice alters the ability of MPs to initiate immune responses against harmful antigens during epididymitis.

Materials and methods

Biological materials

$CX3CR1^{EGFP/+}$ heterozygous (HET) and $CX3CR1^{EGFP/EGFP}$ homozygous (KO) male mice (12–16-week-old) were housed at the Massachusetts General Hospital (MGH) animal facility. In these transgenic mice, one or both copies of the chemokine receptor *Cx3cr1* gene were replaced with enhanced green fluorescent protein (*Egfp*) reporter gene [37]. Consequently, MPs of the HET mice (control) express both *Cx3cr1* and *Egfp* genes, whereas MPs of the KO mice express *Egfp* and are CX3CR1-deficient [4, 5, 37]. The animal procedures were performed based on the National Institutes of Health (NIH) Guide for the Care and Use of Laboratory Animals and approved by the MGH Subcommittee on Research Animal Care. Mice were euthanized with CO_2 (high flow rate) or with isoflurane (2%, mixed with oxygen, Baxter, Deerfield, IL), followed by cervical dislocation.

Ovalbumin injection

Tail vein injection of ovalbumin-Alexa Fluor 647 (OVA; 2 mg/kg; Life Technologies Corporation, Eugene, OR) was performed as previously described [1, 2, 38]. Mice were euthanized 1 h after the OVA challenge. The epididymides were removed and OVA capture was evaluated by flow cytometry and confocal microscopy, as was previously reported [1, 2, 38].

Animal model of epididymitis

Intravasal–epididymal injections with saline (control) or with lipopolysaccharide (LPS; 1 mg/ml endotoxin units, 25 µg) were performed in both epididymides (bilateral) as previously described [14, 15, 39]. LPS was isolated and purified from *Escherichia Coli* O55:B5, S-type (smooth/wild-type) (purity ≥ 99.9%; Innaxon, Oakield Close, UK). Mice were anesthetized with isoflurane and bilateral single incisions were performed to expose the cauda region of the epididymis and the vas deferens (adjacent to the cauda). 25 µl of saline (control) or LPS were injected into the vas deferens lumen, near the cauda, in a retrograde direction using a 31-G needle. Post-surgical pain treatment included the administration of buprenorphine (s.c., 0.1 mg/kg) and bupivacaine (Marcaine; s.c., 8 mg/kg; 0.25%). 48 h after injections, mice were euthanized and the epididymides were

removed and examined by flow cytometry, confocal microscopy, and histological analyses.

Confocal microscopy

Epididymides from CX3CR1$^{EGFP/+}$ HET and CX3CR1$^{EGFP/EGFP}$ KO mice were removed and fixed for 4 h by immersion in 4% paraformaldehyde (PFA) at room temperature. After several washes in phosphate-buffered saline (PBS), the epididymides were soaked in 30% sucrose in PBS (with 0.02% NaAzide) for 48 h at 4 °C. Then, the tissues were embedded in Tissue-Tek OCT compound (Sakura Finetek, Torrance, CA, USA), and frozen on a cutting block in a Reichert Frigocut microtome. Epididymides were cut at 10- or 25-µm thickness and sections were placed onto Fisherbrand Superfrost Plus microscope slides (Fisher Scientific, Pittsburgh, PA, USA).

Immunofluorescence (IF) was performed as we previously reported [1, 40]. For antigen retrieval, the slides were treated with PBS containing 1% SDS and 0.1% Triton for 4 min for all the incubations except for the cleaved caspase-3 staining, which was performed only with PBS containing 1% SDS for 4 min [41]. The antibody against connexin 43 required an additional antigen retrieval step, and slides were microwaved for 1 min (twice for 30 s, separated by 5 min) in 1 mM EDTA, and 10 mM Tris (pH 9.0). Slides were blocked for 1 h at room temperature in PBS containing 1% bovine serum albumin and incubated with the primary antibodies for 18 h at 4 °C. The primary antibodies used were rat monoclonal antibody against F4/80 (20 µg/mL; clone BM8, 14–4801, eBioscience, San Diego, CA), goat polyclonal antibody against integrin alpha E/CD103 (4 µg/mL; AF1990, R&D Systems, Minneapolis, MN), rabbit polyclonal antibody against connexin 43 (gap junction alpha-1 protein (Gja1)) (8 µg/mL; sc-9059, Santa Cruz Biotechnology, Santa Cruz, CA), rabbit monoclonal antibody against cleaved caspase-3 (ASP175) (5A1E) (1:100; #9664, Cell Signaling Technology, Danvers, MA) [42], rabbit polyclonal antibody against AQP9 (0.5 µg/mL; made and purified in the Breton lab [43]), and chicken polyclonal antibody against the V-ATPase B1 subunit (0.3 µg/mL; made and purified in the Breton lab [44]). The secondary antibodies (Jackson ImmunoResearch Laboratories, West Grove, PA) used were donkey Cy3-conjugated anti-rat IgG (3 µg/ml; 712–166–153), donkey Cy3-conjugated anti-goat IgG (1.5 µg/ml; 705–166–147), donkey Alexa Fluor 647-conjugated anti-rabbit IgG (1.5 µg/ml; 711–606–152), donkey Cy3-conjugated anti-chicken IgY (7.5 µg/ml; 703–165–155), and donkey Cy3-conjugated anti-rabbit IgG (7.5 µg/ml; 711–165–152). All antibodies were diluted in DAKO medium (Dako, Carpinteria, CA). Slides were mounted with SlowFade Diamond Antifade Mounting medium (Thermo Fisher Scientific, Waltham, MA) containing the DNA marker DAPI.

For immunostaining negative controls, incubations were achieved with secondary antibodies alone (Suppl. Figure 1a,c–f). Moreover, epididymides from WT mice were used to establish negative fluorescent signals for EGFP and Alexa Fluor 647 (OVA), epididymides from WT mice injected with OVA were used to define positive fluorescent signals for Alexa Fluor 647 and negative signals for EGFP, and epididymides from CX3CR1$^{EGFP/+}$ HET mice without OVA injection were examined to determine negative signals for Alexa Fluor 647 and positive signals for EGFP (Suppl. Figure 1b).

Images were taken using an LSM800 confocal microscope (Zeiss Laboratories, Thornwood, NY) at the Microscopy Core of the Program in Membrane Biology (PMB, MGH, Boston, MA), and using a Nikon CSA-W1 SoRa spinning disk confocal microscope (Nikon, Yokogawa Electric Corporation, Tokyo, Japan) at the Molecular Imaging Core (MGH, Charlestown, MA). 3D reconstructions from Z-stack confocal images were performed with Volocity software (Quorum Technologies Inc., Puslinch, ON).

The number of EGFP$^+$ luminal projections per area of tissue (34,200 µm^2 for Fig. 1c; 39,600 µm^2 for Suppl. Figure 6c) was evaluated using Fiji software. The number of apoptotic cells per area of tissue (39,600 µm^2) was quantified by counting the number of cleaved caspase-3 positive cells in the cauda. The number of damaged epithelial sites was assessed by quantifying morphological alterations in cauda epididymides immunolabeled with epithelial markers (AQP9 and V-ATPase B1 subunit), normalized per area (µm^2) of tissue. Quantifications were performed in at least six mice from each genotype by 2 researchers who were blinded to the experiments. Each image quantification is represented as a dot in the Scatter Dot plot.

Histological evaluation

Hematoxylin and eosin staining was used to evaluate overall morphology. Sections (10 µm) were stained using Hematoxylin Solution, Harris Modified (HHS32, Sigma-Aldrich, St. Louis, MO), and counterstained using Eosin Y Solution (HT110132, Sigma-Aldrich). After staining, the sections were dehydrated, cleared, and coverslipped with Permount mounting medium (SP15-100, Fisher Scientific). Slides were scanned by a digital scanner NanoZoomer 2.0RS (Hamamatsu, Japan) and evaluated by 2 investigators who were blinded to the study.

Flow cytometry analysis

Epididymides from CX3CR1$^{EGFP/+}$ HET and CX3CR1$^{EGFP/EGFP}$ KO mice were removed, and single-cell suspensions were made as we previously described [1]. Briefly, the epididymides were divided into IS, caput/corpus, and cauda

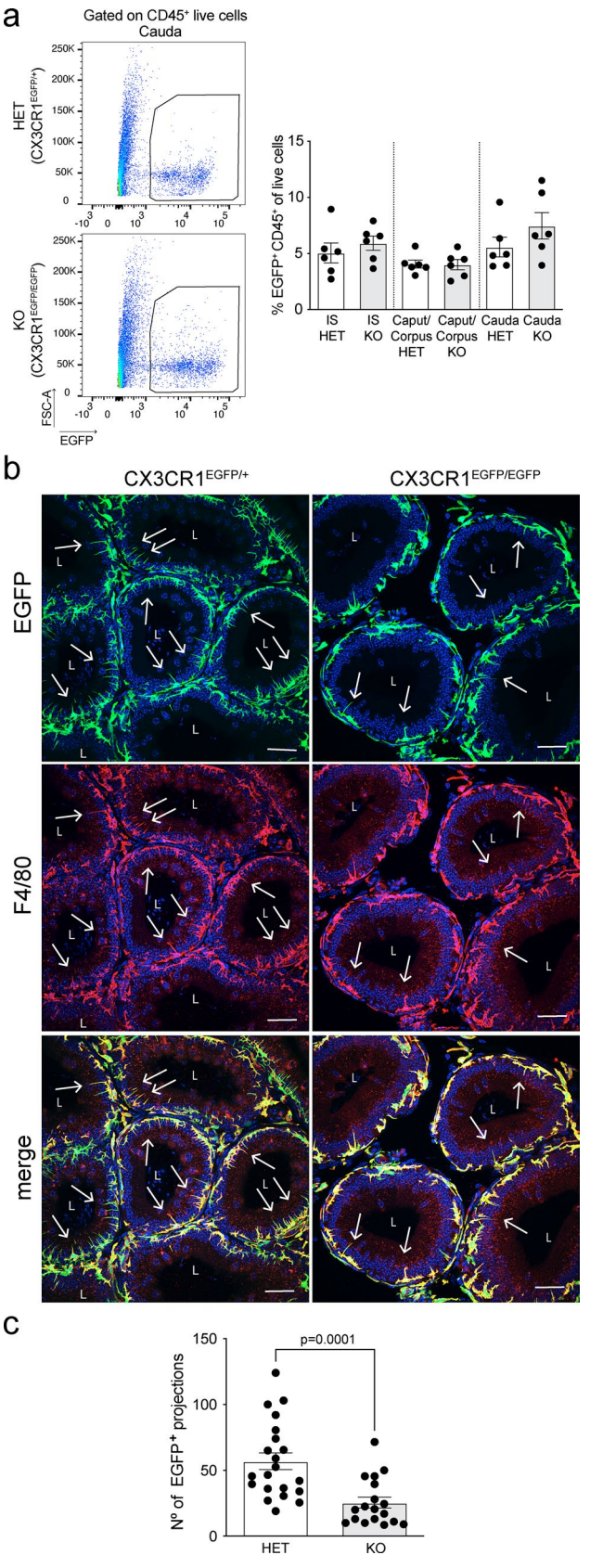

Fig. 1 Characterization of MPs and their luminal projections in the epididymis of CX3CR1$^{EGFP/EGFP}$ KO mice. **a** Flow cytometry analysis of the abundance of EGFP^{+}CD45^{+} MPs in the initial segments (IS), caput/corpus, and cauda epididymis of CX3CR1$^{EGFP/+}$ HET and CX3CR1$^{EGFP/EGFP}$ KO mice. CX3CR1$^{EGFP/+}$ HET mice (control) express both *Cx3cr1* and *Egfp* genes, while CX3CR1$^{EGFP/EGFP}$ KO mice express *Egfp* but lack *Cx3cr1*. We observed a similar abundance of EGFP^{+} MPs between HET and KO mice. Each dot represents a pool of 2 IS, 2 caput/corpus, or 2 cauda regions from each mouse. Data from each epididymal region were analyzed using Student's *t*-test. Data are shown as means ± SEM. **b** Confocal microscopy images showing EGFP^{+} MPs (green) and their luminal projections (arrows) in epididymal IS of CX3CR1$^{EGFP/+}$ HET and CX3CR1$^{EGFP/EGFP}$ KO mice. Tissues are co-labeled with the F4/80 macrophage marker. Nuclei are labeled with DAPI (blue). Bars: 20 µm. *L* lumen. **c** Quantification of the number of EGFP^{+} luminal projections in epididymal IS of CX3CR1$^{EGFP/+}$ HET and CX3CR1$^{EGFP/EGFP}$ KO mice per area of tissue (34,200 µm^2). A decrease in the number of EGFP^{+} luminal projections was observed in the IS of CX3CR1$^{EGFP/EGFP}$ KO mice, compared to CX3CR1$^{EGFP/+}$ HET mice. Each image quantification is represented as a dot. Data were analyzed using the non-parametric Mann–Whitney test. Data are shown as means ± SEM

regions, and tissues were incubated for 30 min at 37 °C with gentle shaking (interval mix of 10 s/min at 1400 rpm) in a dissociation medium containing RPMI 1640 with collagenase type I (0.5 mg/mL) and collagenase type II (0.5 mg/mL). After enzymatic digestion, the cell suspensions were passed through a 70 µm nylon mesh strainer, washed with 2% fetal bovine serum (FBS) containing 2 mM EDTA in PBS, and centrifuged for 5 min at 400 g. Cell suspensions were incubated with different cocktails of anti-mouse antibodies (0.8 µg/mL for each one) against Ly6C R718 (Clone AL-21; 566,987, BD Biosciences, San Jose, CA), CD45 Brilliant Violet 711 (Clone 30-F11; 563,709, BD Biosciences), F4/80 PE/Cyanine 7 (Clone BM8; 123,113, Biolegend, San Diego, CA), CD64 Alexa Fluor 647 (Clone X54-5/7.1; 558,539, BD Biosciences), CD64 Brilliant Violet 786 (Clone X54-5/7.1; 741,024, BD Biosciences), CD11b APC/Cyanine 7 (Clone M1-70; 101,225, Biolegend), MHC Class II (I-A/I-E) PE (Clone M5/114.15.2; 12-5321-81, Invitrogen, Carlsbad, CA), CD103 Brilliant Violet 786 (Clone M290; 564,322, BD Biosciences), which were diluted in 2% FBS in PBS containing BD Horizon Brilliant Stain buffer (BD Biosciences). After 30 min, cells were washed in 2% FBS in PBS and passed through a 40 µm cell strainer. Flow cytometry analyses were performed at the HSCI-CRM Flow Cytometry Core (Boston, MA). DAPI was used as the viability dye for flow cytometry analyses. Data were acquired on a BD FACSAria II flow cytometer (BD Biosciences) and analyzed using FlowJo software version 10.8.1 (BD Biosciences).

For the negative controls, epididymides from WT mice were analyzed to define negative fluorescent signals for EGFP (Suppl. Figure 3a). For the assessment of OVA (Alexa Fluor 647) capture, additional controls included

epididymides from WT mice to establish negative signals for EGFP and Alexa Fluor 647, epididymides from WT mice injected with OVA to determine positive signals for Alexa Fluor 647 and negative signals for EGFP, and epididymides from CX3CR1$^{EGFP/+}$ HET mice without OVA injection to establish negative signals for Alexa Fluor 647 and positive signals for EGFP (Suppl. Figure 3b).

For the immunophenotype analysis, FMO (fluorescence minus one; Suppl. Figure 2) and negative (Suppl. Figure 3) controls were performed to determine the gating strategies. Each FMO control includes all antibodies involved in the experiment, except one [45]. For the negative control, epididymal cells were not stained with any antibody.

Isolation of EGFP$^+$ MPs, RNA extraction, and qPCR

Isolation of EGFP$^+$ MPs from the epididymides of CX3CR1$^{EGFP/+}$ HET and CX3CR1$^{EGFP/EGFP}$ KO mice was performed as previously described [1]. Epididymal single-cell suspensions were generated as explained above. Fluorescence-activated cell sorting (FACS) was performed at the HSCI-CRM Flow Cytometry Core (Boston, MA) on a BD FACSAria II flow cytometer (BD Biosciences) under low-pressure conditions (100 µm Nozzle) and using the Purity precision mode. DAPI was used as a viability dye. Live EGFP$^+$ single cells were sorted at low pressure, and RNA was isolated using the PicoPure RNA Isolation Kit (ARCTURUS PicoPure RNA Extraction Buffer, Applied Biosystems, Waltham, MA), following the manufacturer's instructions. For the removal of genomic DNA contamination, RNA samples were treated with the RNase-free DNase set (Qiagen, Hilden, Germany). The total amount and quality of RNA were measured by the Agilent RNA 6000 Pico Kit (Agilent Technologies, Waldbronn, Germany) using the Agilent 2100 Bioanalyzer instrument (Agilent Technologies). cDNA was synthesized from 1000 pg RNA using the SuperScript VILO cDNA Synthesis Kit (11754–050, Invitrogen) according to the manufacturer's instructions. Quantitative PCR (qPCR) was performed using the Power SYBR Green PCR Master Mix (A25742, Thermo Fisher Scientific, Waltham, MA). The primers used are listed in Suppl. Table I. Results are reported as mean ± SEM using the formula $-\Delta Ct = -$[Ct target *Gja1* gene–Ct housekeeping gene *Gapdh*]. Relative expression is derived from $2^{-\Delta\Delta Ct}$, where $-\Delta\Delta Ct = \Delta Ct$ epididymal sample – mean of ΔCt control group (HET).

Statistical analysis

Data analysis was performed using GraphPad Prism version 9.4.0 (GraphPad Software, La Jolla, CA, www.graphpad.com). To examine if the samples were normally distributed, we performed a test of normality (Shapiro–Wilk test) and an analysis of variance (*F* test to compare two groups or Bartlett's test (corrected) to compare three or more groups). Student's *t*-test (two-tailed) or one-way ANOVA followed by Tukey's post hoc tests were used as parametric tests. Mann–Whitney test (two-tailed) or the Kruskal–Wallis test followed by Dunn's post hoc test were used as non-parametric tests. *P*-values < 0.05 were determined statistically significant. Data were expressed as the means ± SEM. For each dataset, at least six different mice were examined per condition.

Results

Morphological and immunophenotypical switch in CX3CR1-deficient MPs

To characterize the role of CX3CR1 in the recognition of sperm cells and pathogens within the epididymis, we used transgenic mice in which one or both copies of the chemokine receptor *Cx3cr1* gene was replaced with enhanced green fluorescent protein (*Egfp*) reporter gene [37]. In these mice, *Egfp* expression is under the control of the CX3CR1 promoter and, consequently, the MPs of the heterozygous mice (CX3CR1$^{EGFP/+}$, HET; control) express both *Cx3cr1* and *Egfp* genes, whereas MPs of the homozygous (CX3CR1$^{EGFP/EGFP}$, KO) mice express *Egfp* and are CX3CR1-deficient. First, by flow cytometry, we found that the IS, caput/corpus, and cauda of CX3CR1$^{EGFP/+}$ HET and CX3CR1$^{EGFP/EGFP}$ KO mice showed a similar abundance of EGFP$^+$ MPs (Fig. 1a). Interestingly, using confocal microscopy, we observed a significant decrease in the number of luminal reaching projections of EGFP$^+$ MPs in CX3CR1$^{EGFP/EGFP}$ KO mice, compared to the CX3CR1$^{EGFP/+}$ HET mice (Fig. 1b, c). Most of the CX3CR1-deficient and HET MPs were co-labeled with the F4/80 macrophage marker (Fig. 1b). Despite the KO MPs presenting fewer luminal reaching projections, 3D confocal microscopy showed that these projections are still in close interaction with epididymal epithelial CCs (Video 1), indicating that both cell types are strategically positioned to have a role in epididymal mucosa immunity. The epididymis is populated by diverse subsets of MPs that express a combination of surface molecules traditionally described as "dendritic cell" (DC), "macrophage" or "monocyte" markers [1–3, 12, 33]. Flow cytometry analysis revealed no differences in the number of epididymal EGFP$^+$ MPs expressing macrophage (F4/80$^+$CD11b$^+$CD45$^+$, Fig. 2a) or DC markers (MHCII$^+$CD64$^-$CD11b$^+$CD45$^+$, Fig. 2b) between CX3CR1$^{EGFP/EGFP}$ KO and CX3CR1$^{EGFP/+}$ HET mice. However, a reduction of EGFP$^+$ MPs with a monocytic phenotype (Ly6C$^+$MHCII$^-$CD64$^-$CD11b$^+$CD45$^+$ cells, Fig. 2c)

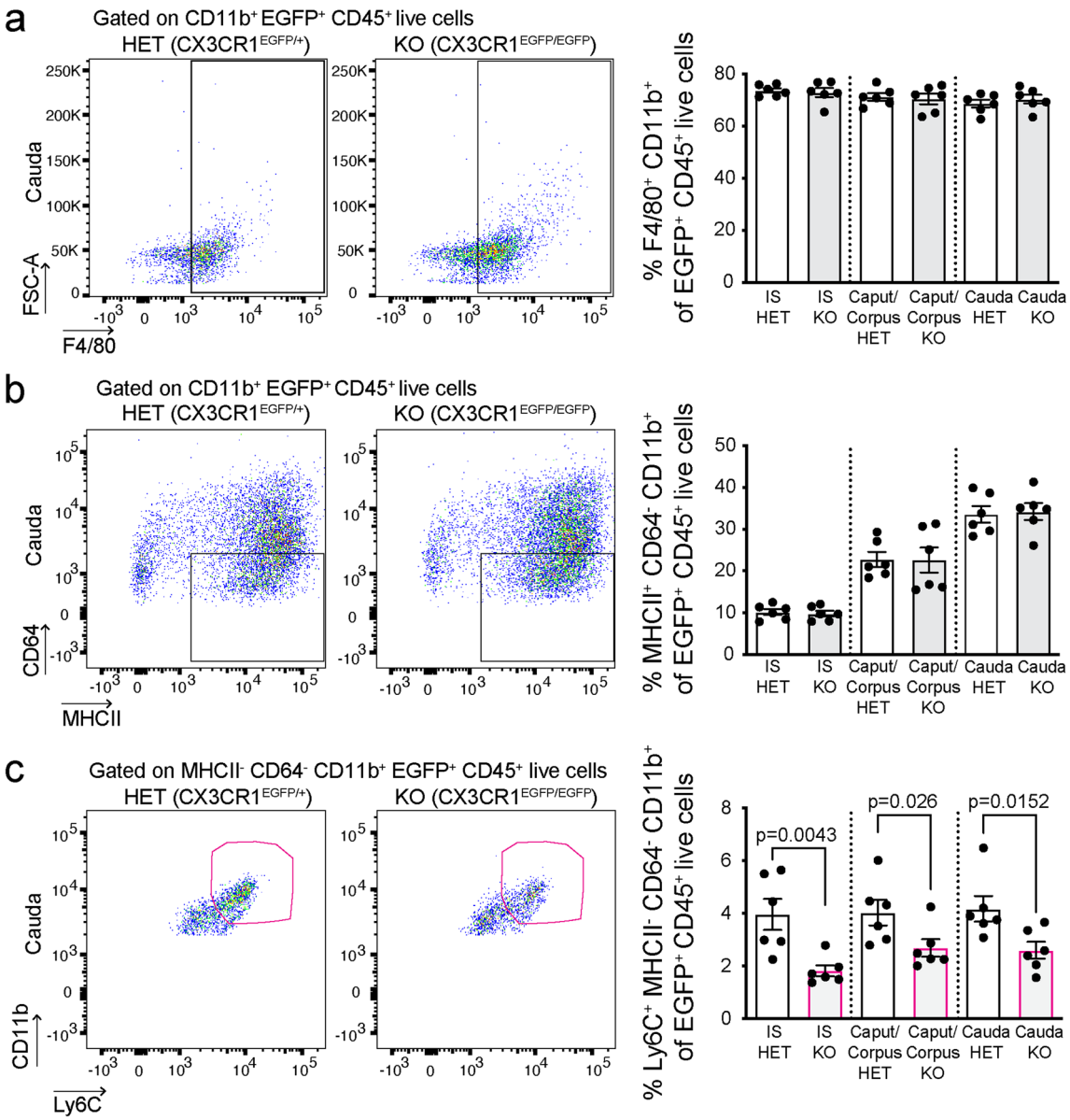

Fig. 2 CX3CR1$^{EGFP/EGFP}$ KO MPs have a reduced monocytic phenotype under physiological conditions. Flow cytometry analysis of EGFP$^+$ MPs with a macrophage (F4/80$^+$CD11b$^+$CD45$^+$) (**a**), MHCII$^+$ dendritic cell (DC) (MHCII$^+$CD64$^-$CD11b$^+$CD45$^+$) (**b**), or monocyte (Ly6C$^+$MHCII$^-$CD64$^-$CD11b$^+$CD45$^+$) (**c**) profile in IS, caput/corpus and cauda epididymis of CX3CR1$^{EGFP/+}$ HET and CX3CR1$^{EGFP/EGFP}$ KO mice. Each dot represents a pool of 2 IS, 2 caput/corpus, or 2 cauda regions from each mouse. Data from each epididymal region were analyzed using Student's *t*-test (**a**, **b**) or the non-parametric Mann–Whitney test (**c**). Data are shown as means ± SEM

was observed in the CX3CR1$^{EGFP/EGFP}$ KO epididymis (Fig. 2c) under physiological conditions.

CX3CR1 deficiency affects the functional properties of epididymal MPs

To assess whether the absence of CX3CR1 could impact

the uptake of circulatory antigens in the epididymis, mice were injected intravenously with fluorescent antigens (ovalbumin (OVA)-Alexa Fluor 647) into CX3CR1$^{EGFP/+}$ HET and CX3CR1$^{EGFP/EGFP}$ KO mice. The capture activity of CX3CR1$^{EGFP/+}$ HET and CX3CR1$^{EGFP/EGFP}$ KO MPs was evaluated by flow cytometry 1 h after the injection. No apparent overall impairment in the internalization of OVA was observed in KO MPs from IS (Fig. 3a), caput/corpus (Suppl. Figure 4a), and cauda regions (Suppl. Figure 4b). Confocal microscopy showed that several interstitial EGFP$^+$ MPs (Fig. 3b; green, arrowhead) and intraepithelial EGFP$^+$ MPs (Fig. 3b; green, arrows) internalized OVA (red) in the IS of CX3CR1$^{EGFP/+}$ HET mice. However, we revealed a reduction in antigen capture specifically in intraepithelial EGFP$^+$ MPs and their luminal projections in the IS of the CX3CR1$^{EGFP/EGFP}$ KO mice, compared to CX3CR1$^{EGFP/+}$ HET mice (Fig. 3b, arrows). The discrepancy in OVA capture between flow cytometry and IF analyses could be because interstitial and intraepithelial MPs were studied together by flow cytometry, masking the OVA capture deficiency of intraepithelial EGFP$^+$ KO MPs. Furthermore, flow cytometry showed that EGFP$^+$ MPs that internalized OVA in the IS of CX3CR1$^{EGFP/EGFP}$ KO mice exhibited a reduced macrophage profile (CD64$^+$CD11b$^+$CD45$^+$ (Fig. 3c)) *versus* CX3CR1$^{EGFP/+}$ HET mice. However, this reduction of EGFP$^+$OVA$^+$ MPs with macrophage profile was not observed in the cauda of CX3CR1$^{EGFP/EGFP}$ KO mice (Suppl. Figure 5a). Also, using confocal microscopy, no difference in OVA capture was observed in the more distal epididymal regions between CX3CR1$^{EGFP/+}$ HET and CX3CR1$^{EGFP/EGFP}$ KO mice (Suppl. Figure 5b).

To study the role of CX3CR1 in the epididymal immune response against bacterial antigens, CX3CR1$^{EGFP/EGFP}$ KO and CX3CR1$^{EGFP/+}$ HET mice were subjected to intravasal-epididymal luminal injection with ultra-purified LPS from *Escherichia coli* or with saline. Non-injected mice were used as controls. After saline or LPS injections, flow cytometry showed differences in the response of the cauda EGFP$^+$ MPs from CX3CR1$^{EGFP/EGFP}$ KO *versus* CX3CR1$^{EGFP/+}$ HET mice. In the HET mice, injection of either saline or LPS resulted in a significant reduction in the abundance of cauda EGFP$^+$ HET MPs, compared with non-injected mice, and the percentage of EGFP$^+$ HET MPs did not differ between saline- and LPS-treated epididymides (Fig. 4a). This result indicates that the intravasal–epididymal injection per se produces changes in the immune cell populations in HET animals. Indeed, we previously reported that a significant neutrophil and monocyte infiltration occurs upon intravasal–epididymal saline injection [14]. However, in the CX3CR1$^{EGFP/EGFP}$ KO mice, the reduction in the abundance of cauda EGFP$^+$ KO MPs was only observed after LPS injections, and no differences in the EGFP$^+$ KO MP population were observed between non-injected and saline-injected epididymides (Fig. 4a). This remarkable difference between HET and KO MPs suggests that in the absence of CX3CR1, EGFP$^+$ KO MPs display impairment in the response to surgery-induced injury. Confocal microscopy confirmed flow cytometry data showing the decrease of EGFP$^+$ KO MPs after LPS injection compared to the saline group in the cauda of CX3CR1-deficient mice (Fig. 4b). Moreover, flow cytometry analysis revealed a switch in the immunophenotypic profile of cauda EGFP$^+$ KO MPs after LPS injection: a reduction in EGFP$^+$ KO MPs with a macrophage phenotype (MHCII$^+$CD64$^+$CD11b$^+$CD45$^+$, Fig. 4c) together with an increase in EGFP$^+$ KO MPs with a monocytic signature (Ly6C$^+$MHCII$^-$CD64$^-$CD11b$^+$CD45$^+$, Fig. 4d). In contrast to the cauda, in the IS, the number of epididymal EGFP$^+$ MPs remained unaltered between saline- and LPS-injected groups from KO and HET mice (Fig. 1a, Suppl. Figure 6a). Intriguingly, the luminal-reaching protrusions of EGFP$^+$ MPs (Suppl. Figure 6b; green; arrows) were reduced in HET mice after LPS injection compared to saline injection, while no difference was observed in the EGFP$^+$ KO MPs (Suppl. Figure 6b-c). The lack of reduction in the luminal protrusions observed in the EGFP$^+$ KO MPs after LPS injection could be explained because, at steady-state, the CX3CR1-deficient MPs display the lowest number of luminal projections (Fig. 1b, c), and they might not be further reduced by LPS.

The absence of CX3CR1 results in impaired communication between MPs and CD103$^+$ dendritic cells (DCs)

It is known that CX3CR1$^+$ MPs do not present antigens primarily because they quickly transfer them to adjacent CD103$^+$ DCs, which are proficient in antigen presentation [46, 47]. Surprisingly, using flow cytometry, we found an accumulation of CD103$^+$CD11b$^+$DCs in the caput/corpus (Fig. 5a) and cauda epididymis (Fig. 5b) of CX3CR1$^{EGFP/EGFP}$ KO mice, but not in CX3CR1$^{EGFP/+}$ HET animals, 48 h after the LPS challenge. Subsets of tissue DCs express CD103 in the epididymis [1, 4] as well as in other organ systems [48]. In addition, IF studies confirmed the accumulation of CD103$^+$ cells (red) in the epididymal interstitium after LPS injection, *versus* saline injection, in the corpus and cauda of CX3CR1$^{EGFP/EGFP}$ KO mice (Fig. 5c), supporting the flow cytometry results. These findings suggest that the deletion of CX3CR1 affects antigen capture and transfer to CD103$^+$ DCs. Consequently, these DCs might not migrate to the lymph nodes to mount an immune response against infection and might accumulate in the epididymis.

Gap junctions (GJs) are channels that allow intercellular communication, and their major constituents are connexin proteins [49, 50]. We have previously reported that epididymal MPs mostly expressed connexin 43 (*Gja1*) [1],

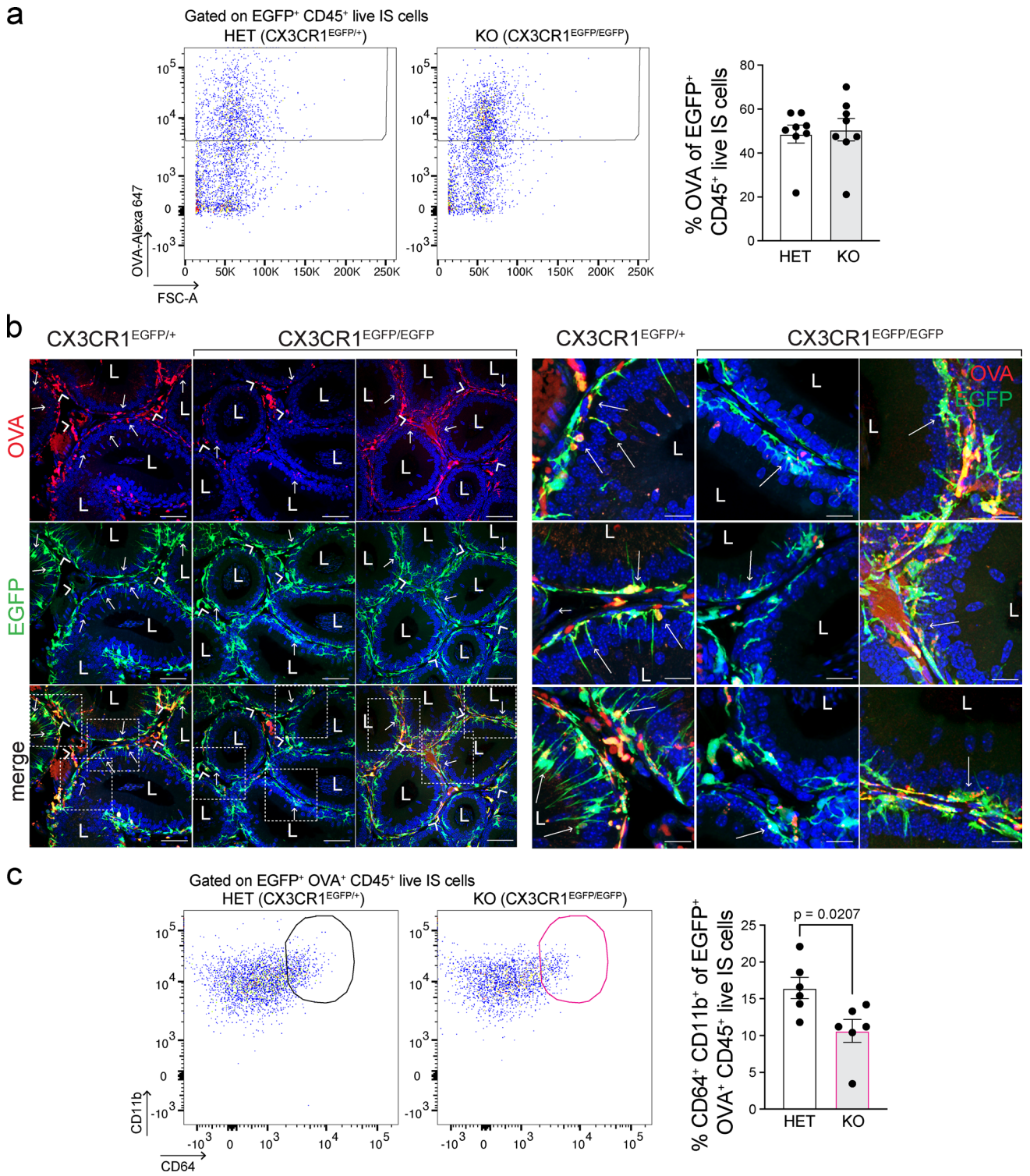

a GJ protein that is required for effective antigen transfer from MPs to CD103$^+$ DCs in the intestine [47]. Interestingly, we found downregulation of *Gja1* (connexin 43) expression in sorted epididymal EGFP$^+$ KO MPs compared to EGFP$^+$ HET MPs by qPCR analysis (Fig. 6a). Furthermore, we revealed close interactions (dashed white squares) between EGFP$^+$ MPs (green) and CD103$^+$ DCs (pink) in CX3CR1$^{EGFP/+}$ HET (Fig. 6b, panel *i*; Videos 2, 3 and 4) and in CX3CR1$^{EGFP/EGFP}$ KO epididymides (Fig. 6b, panel *ii*; Videos 5 and 6). 3D confocal microscopy images showed that EGFP$^+$ HET MPs (green) and CD103$^+$ DCs (pink) had points of interaction marked by the GJ protein connexin 43

◂**Fig. 3** Altered capture activity of circulating antigens by CX3CR1-deficient MPs. Circulatory antigens (ovalbumin-Alexa 647 (OVA); 2 mg/kg) were injected through tail vein injection into CX3CR1$^{EGFP/+}$ HET and CX3CR1$^{EGFP/EGFP}$ KO mice, and antigen capture was assessed 1 h after injections. **a** Flow cytometry analysis of EGFP$^+$ MPs that internalized fluorescent OVA in IS of HET and KO mice. Flow cytometry analysis of caput/corpus and cauda regions is shown in Suppl. Figure 4. Overall, we observed similar OVA internalization by epididymal MPs in HET and KO mice in all epididymal regions. **b** Confocal microscopy images showing EGFP$^+$ (green) OVA$^+$ (red) cells in the IS of CX3CR1$^{EGFP/+}$ HET and CX3CR1$^{EGFP/EGFP}$ KO mice. In the IS of the HET mice, several interstitial EGFP$^+$ MPs (arrowheads) and intraepithelial EGFP$^+$ MPs (arrows) internalized circulating OVA. A reduced OVA capture by intraepithelial KO MPs and their luminal projections was observed in the IS of the KO mice. The right panel shows higher magnifications of the regions delineated by the white boxes in the bottom left panel. Nuclei are labeled with DAPI (blue). Bars (left panel): 50 µm, Bars (right panel; magnifications): 10 µm. *L* lumen. **c** Flow cytometry analysis of EGFP$^+$ MPs that internalized OVA and display macrophage profile (CD64$^+$CD11b$^+$CD45$^+$) in IS of HET and KO mice. The percentage of EGFP$^+$ OVA$^+$ KO MPs with a macrophage signature was significantly reduced compared to EGFP$^+$ OVA$^+$ HET MPs. Each dot represents a pool of 2 IS from each mouse. Data from each IS were analyzed using the non-parametric Mann–Whitney test (**a**) and Student's *t*-test (**c**). Data are shown as means ± SEM

(Cx43; red) in CX3CR1$^{EGFP/+}$ HET epididymides (Fig. 6b, arrows in panel *i*; Videos 3 and 4). Single Z-stack planes (Suppl. Figure 7a) of the 3D images displayed in Fig. 6b*i* show the sites of interaction (arrows) between EGFP$^+$ MPs (green) and CD103$^+$ cells (pink) by the GJ protein connexin 43 (Cx43; red) in the epididymides of CX3CR1$^{EGFP/+}$ HET mice. However, no apparent connexin 43 staining was detected at the cell–cell interaction sites between EGFP$^+$ KO MPs and CD103$^+$ cells in the CX3CR1$^{EGFP/EGFP}$ KO epididymides (Fig. 6b, panel *ii*; Videos 5 and 6).

The lack of CX3CR1 affects epididymal epithelium upon infection

To investigate whether the immunological defects observed in HET and KO epididymides were associated with changes in tissue morphology, we assessed the state of the epididymal epithelium of CX3CR1$^{EGFP/+}$ HET and CX3CR1$^{EGFP/EGFP}$ KO mice 48 h after LPS or saline injections. Sections of cauda epididymides were stained with antibodies that detect the B1 subunit of the V-ATPase (a marker of CCs) and aquaporin 9 (AQP9; a marker of principal cells). Both saline- and LPS-injected epididymides presented a large portion of epithelial damage in the CX3CR1$^{EGFP/+}$ HET *versus* CX3CR1$^{EGFP/EGFP}$ KO mice (Fig. 7a (arrows), 7b). Noticeably, we observed that the affected areas in the cauda of HET mice after LPS injections were more severely damaged compared to saline-injected HET cauda (Fig. 7a, arrows). These observations show the presence of epididymal epithelium defects in CX3CR1$^{EGFP/+}$ HET mice from both LPS and saline-injected groups, with a stronger phenotype in LPS-injected males. Additionally, we observed the absence of rows of CCs in all the groups except in the saline-injected CX3CR1$^{EGFP/EGFP}$ KO epididymides. Histological evaluation by hematoxylin and eosin (HE) staining confirmed that epithelial damage was induced in cauda of CX3CR1$^{EGFP/+}$ HET mice after LPS or saline injections, compared to CX3CR1$^{EGFP/EGFP}$ KO mice (Suppl. Figure 8). Altogether, our results suggest that the lack of CX3CR1 in the epididymis attenuates epididymal damage 48 h after the LPS challenge. The latter is supported by our results showing reduced numbers of cleaved caspase-3 (apoptotic) cells after LPS injection in the CX3CR1$^{EGFP/EGFP}$ KO *versus* CX3CR1$^{EGFP/+}$ HET mice, as well as in the saline-injected mice (Fig. 7c, d).

Taken together, in our working model (Fig. 8), upon infection, epididymal cells communicate through proinflammatory chemokines/cytokines with strategically tissue-located MPs to mount a bacterial-associated response [14–16, 39]. This is then followed by the rapid recruitment of monocytes [1, 3, 15, 17, 35] that might differentiate into CD103$^+$ DCs [51–53]. Epididymal resident CD103$^+$ cells may also proliferate in response to infection. CX3CR1$^+$ MPs take up antigens ([1] and this study) and it is possible that these cells quickly transfer the information to adjacent CD103$^+$ DCs, which may migrate to lymph nodes and could facilitate a local inflammatory response that contributes to the injury [46, 47, 54–56]. Our results suggest that this cell–cell communication between CX3CR1$^+$ MPs and CD103$^+$ DCs is mediated by the GJ protein connexin 43. In CX3CR1-deficient epididymis, upon infection, epididymal cells would activate an inflammatory response facilitating the recruitment of monocytes, among other immune cells, to the site of inflammation. However, intraepithelial CX3CR1$^+$ KO MPs show impaired capture activity and might not transfer antigens to CD103$^+$ DCs with the same efficiency as control, presumably due to the downregulation of connexin 43 expression. Thus, CD103$^+$ cells would not migrate to the lymph nodes and would accumulate in the epididymal interstitium. Moreover, deleting the CX3CR1 receptor significantly reduces the impact of the infection by attenuating epididymal tubule damage, probably by blunting the release of inflammatory molecules from EGFP$^+$ KO MPs.

Discussion

Our results address important knowledge gaps by leveraging novel mechanisms by which resident mononuclear phagocytes (MPs) maintain epididymal mucosal homeostasis and have significant implications for our understanding of male

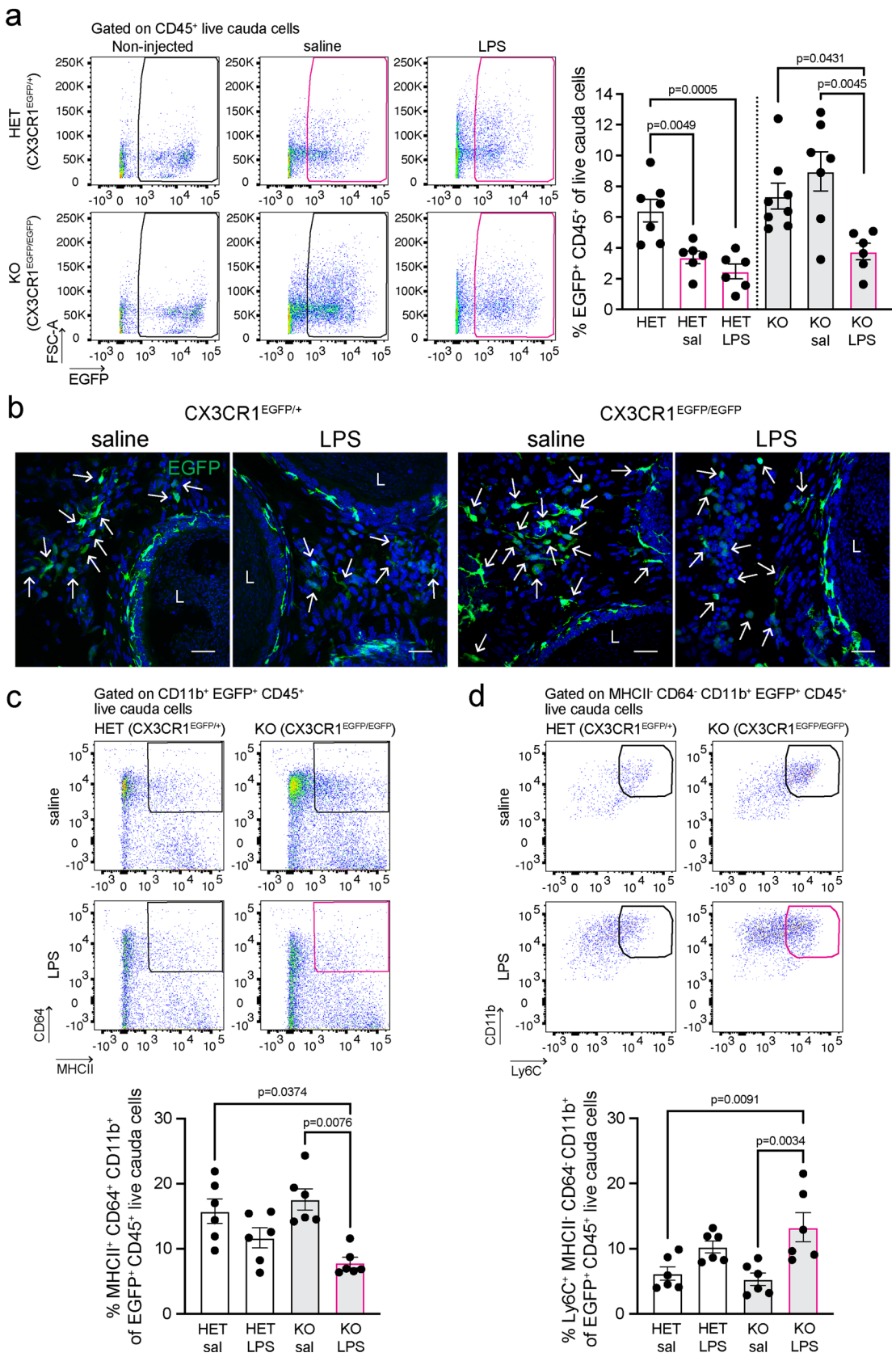
a
Gated on CD45+ live cauda cells
Non-injected
saline
LPS
HET (CX3CR1EGFP/+)
KO (CX3CR1EGFP/EGFP)
FSC-A
EGFP
% EGFP+ CD45+ of live cauda cells
p=0.0005
p=0.0049
p=0.0431
p=0.0045
HET
HET sal
HET LPS
KO
KO sal
KO LPS
b
CX3CR1EGFP/+
CX3CR1EGFP/EGFP
saline
LPS
EGFP
L
c
Gated on CD11b+ EGFP+ CD45+ live cauda cells
HET (CX3CR1EGFP/+)
KO (CX3CR1EGFP/EGFP)
CD64
MHCII
% MHCII+ CD64+ CD11b+ of EGFP+ CD45+ live cauda cells
p=0.0374
p=0.0076
d
Gated on MHCII- CD64- CD11b+ EGFP+ CD45+ live cauda cells
CD11b
Ly6C
% Ly6C+ MHCII- CD64- CD11b+ of EGFP+ CD45+ live cauda cells
p=0.0091
p=0.0034

◂**Fig. 4** The immune response of CX3CR1$^{EGFP/EGFP}$ KO epididymis at 48 h after LPS injection. Immune response was evaluated 48 h after intravasal-epididymal injection of lipopolysaccharide (LPS; 25 µg) from *E. Coli*. Saline (sal) injection was performed for the controls. **a** Flow cytometry analysis of EGFP$^+$ CD45$^+$ MPs in the cauda of CX3CR1$^{EGFP/+}$ HET and CX3CR1$^{EGFP/EGFP}$ KO mice 48 h after injection with saline or LPS. In the HET epididymides, EGFP$^+$ MP percentage decreased after injection of saline or LPS compared to non-injected epididymides (left bar). However, in the KO mice, we observed no significant changes in the percentage of EGFP$^+$ MPs between the saline-treated and non-injected epididymides, and a reduction in the EGFP$^+$ MP abundance between the saline-treated and LPS-treated groups. **b** Confocal microscopy showed that, in the cauda epididymis, there is a similar EGFP$^+$ MP (green) abundance in the interstitium of HET mice after saline or LPS injections, while in the CX3CR1-deficient mice, we observed more interstitial EGFP$^+$ KO MPs in saline-treated compared to LPS-injected cauda. Bars: 20 µm. Nuclei are labeled with DAPI (blue). *L* lumen. Flow cytometry analysis showed a decrease of EGFP$^+$ MPs with a macrophage signature (MHCII$^+$CD64$^+$CD11b$^+$CD45$^+$) (**c**) and an increase of EGFP$^+$ MPs with a monocytic profile (Ly6C$^+$MHCII$^-$CD64$^-$CD11b$^+$CD45$^+$) (**d**) in the cauda epididymis of CX3CR1$^{EGFP/EGFP}$ KO mice after LPS-treatment *versus* control. Each dot represents a pool of 2 cauda regions from each mouse. Data from each cauda were analyzed using one-way ANOVA followed by Tukey's post hoc test (**a, d**) and the non-parametric Kruskal–Wallis test followed by Dunn's post hoc test (**c**). Data are shown as means ± SEM

infertility. We show that MPs from CX3CR1-deficient mice display morphological alterations in their luminal-reaching intraepithelial projections and exhibit impaired particle sampling ability and defective cell–cell crosstalk with CD103$^+$ DCs. In addition, the lack of CX3CR1 in MPs attenuated epididymal epithelial damage following the LPS challenge, revealing cell–cell communication networks between MPs and epithelial cells in the epididymis.

MPs form an intricate network of phagocytes and professional antigen-presenting cells in all epididymal regions [1–4, 14, 33]. This heterogeneous cell population is responsible for the clearance of apoptotic cells and cellular debris in the epididymis, thus maintaining the integrity of the blood–epididymis barrier [5, 13]. Epididymal CX3CR1$^+$ MPs can extend intraepithelial dendrites into the epididymal luminal compartment to sample and capture antigens [1, 2, 14], similar to what was observed in the lumen of the intestine [47, 57, 58]. Here, using CX3CR1$^{EGFP/EGFP}$ KO mice, we show that epididymal EGFP$^+$ KO MPs display a reduction in the number of their dendrites reaching towards the lumen, indicating that the formation of the luminal reaching projections depends on CX3CR1 activation. The reduction in the abundance of MP luminal projections also impairs the oral tolerance to food antigens in the intestine [58, 59], and induces alterations in adult neurogenesis in the olfactory bulb [60, 61].

In addition, we revealed that CX3CR1$^{EGFP/EGFP}$ KO MPs have a reduced monocytic phenotype under physiological conditions compared to control MPs, indicating a central role of this receptor on the tissue monocyte homeostasis. Indeed, CX3CR1 was found to be involved in the migration of blood monocytes into tissues and their phenotypic differentiation [62]. Moreover, we observed a shift in the immunophenotypic profile of EGFP$^+$ KO MPs that take up OVA in the IS as well as after LPS injection in the cauda. These results show that MPs could change the expression of surface markers at different physiopathological states and reveal the involvement of the CX3CR1 signaling pathway in the cellular plasticity of MPs.

We previously identified distinct transcriptomic signatures of EGFP$^+$ MPs isolated from the different epididymal regions of epididymis from CX3CR1$^{EGFP/+}$ HET mice [1]. In the current study, a higher percentage of MPs that had captured antigens was observed in the IS compared to the other epididymal segments in CX3CR1-deficient mice, similar to what we previously found for the CX3CR1$^{EGFP/+}$ HET epididymis [1, 2]. However, we observed that intraepithelial epididymal KO MPs from the proximal regions were devoid of antigens upon OVA challenge. In contrast, in the cauda region, the antigen capture by interstitial CX3CR1-deficient MPs was not affected, but the LPS challenge induced changes in the EGFP$^+$ MP abundance and their phenotype in CX3CR1$^{EGFP/EGFP}$ KO epididymis. These results indicate the region-specific roles of MPs in different immuno-mechanisms and confirm that these heterogeneous cell populations exhibit features that strongly depend on their location and the micro-environment of the epididymis [1, 14, 63, 64].

CX3CR1$^+$ MPs show high dynamic dendrite protrusions to sample luminal antigens, but low migratory activity, and truncated antigen-presenting activity [1, 47, 58, 59]. In contrast, CD103$^+$ DCs are specialized players in antigen cross-presentation with a high migration rate during inflammation [46, 55, 56]. In the intestine, it was found that after antigens are captured by CX3CR1$^+$ MPs, they are quickly transferred to CD103$^+$ DCs through gap junctions via a mechanism that is connexin 43-dependent [47]. Importantly, the authors reported that CX3CR1-deficiency alters this cell–cell crosstalk and induces defects in the establishment of oral tolerance [47]. We found a downregulation of connexin 43 expression in epididymal CX3CR1-deficient MPs, which correlates with the failure of CD103$^+$ DCs to mount immune responses toward antigens. During epididymitis, in the absence of the CX3CR1 signaling pathway in MPs, CD103$^+$ DCs might be unable to acquire antigens and migrate to the lymphoid nodes, resulting in an accumulation of these DCs in the interstitium, as we observed in the CX3CR1$^{EGFP/EGFP}$ KO epididymis. In agreement with this notion, CX3CR1 deficiency was shown to induce DC accumulation in the aorta in aged animals [65]. Interestingly, in the heart, the deletion of connexin 43 in CX3CR1$^+$ macrophages induces alteration in the mouse cardiac conduction system [66]. In addition,

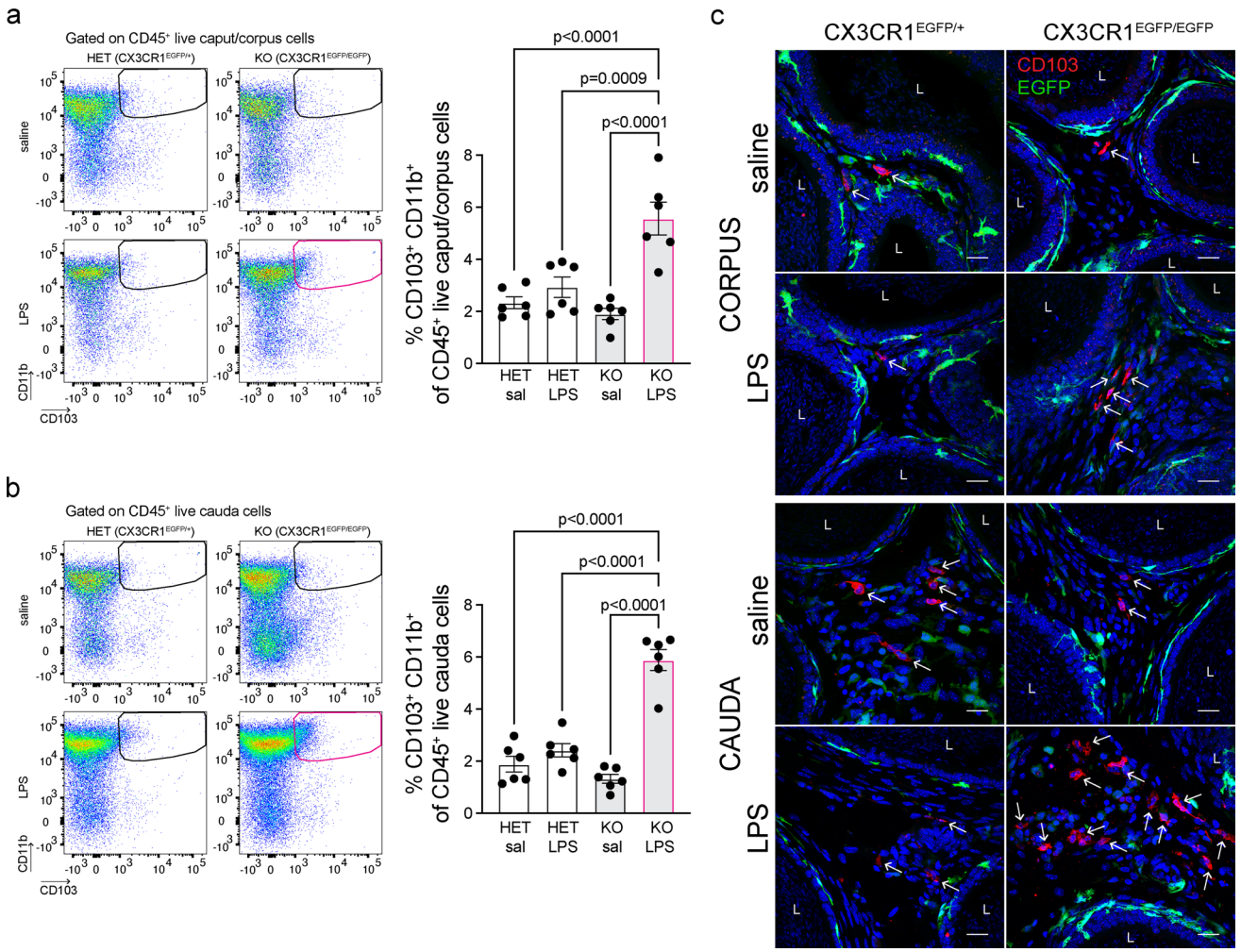

Fig. 5 Accumulation of CD103$^+$ DCs in the CX3CR1$^{EGFP/EGFP}$ KO epididymis after LPS injection. Flow cytometry analysis showed an increase of CD103$^+$ DCs (CD103$^+$CD11b$^+$CD45$^+$) in the caput/corpus (**a**) and cauda epididymis (**b**) of CX3CR1$^{EGFP/EGFP}$ KO mice 48 h after LPS injection, compared to the saline-treated KO group or LPS-injected CX3CR1$^{EGFP/+}$ HET mice. Each dot represents a pool of 2 caput/corpus or 2 cauda regions from each mouse. Data were analyzed using one-way ANOVA followed by Tukey's post hoc test. Data are shown as means ± SEM. **c** Confocal microscopy images showing accumulation of interstitial CD103$^+$ cells (red; arrows) in the corpus (top panels) and cauda (bottom panels) of KO epididymides, compared to HET samples, 48 h after Saline or LPS injection. Nuclei are labeled with DAPI (blue). EGFP$^+$ MPs are shown in green. Bars: 15 µm. *L* lumen

it was recently reported that connexin 43 plays a critical role in establishing cell–cell communication among epididymal epithelial cells [42]. Thus, EGFP$^+$ KO MPs might also present a defective cell–cell crosstalk with epithelial cells and might be unable to mount the appropriate immune response against infection. Indeed, after injections, we observed a reduction in epithelial injury in the CX3CR1$^{EGFP/EGFP}$ KO epididymis, which supports the possibility of defective communication between MPs and epithelial cells.

Epididymitis is an inflammatory condition that frequently induces male infertility [17, 18, 21–27, 67]. Pathogens populate the epididymis via their retrograde ascent through the urethra and there is growing evidence that this damaging process implicates infiltration of circulatory monocytes as well as resident macrophage proliferation [3, 14, 16, 33]. Based on these observations, in our study, the increase in EGFP$^+$ KO MPs with a monocytic signature after LPS injection might be infiltrating from circulation. The strong immunopathological alterations following epididymitis occur in the distal epididymal regions [14, 24, 25, 33]. However, in the proximal segments, immunocytes and epithelial cells can also respond to inflammatory stimuli [14, 24, 25, 33]. During the early phase of the inflammation, CX3CR1$^+$ MPs participate in antigen capture by protruding their dendrites into the lumen, and then they undergo striking morphological and phenotypical changes to be more efficient in transferring the information to other immune cells, such as CD103$^+$

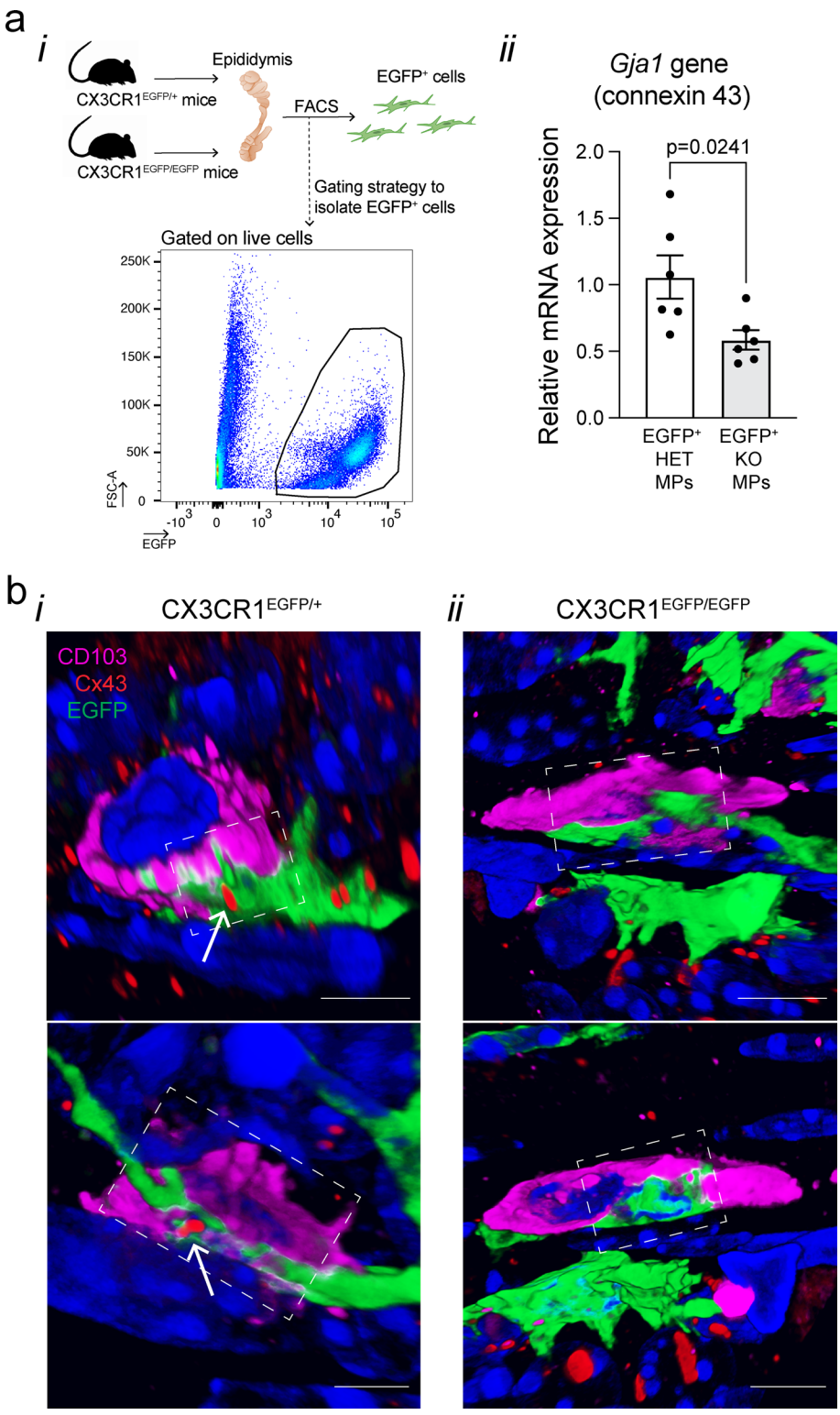

Fig. 6 Impaired expression of *Gja1* (connexin 43) in CX3CR1-deficient MPs. **a** qPCR analysis of *Gja1* expression (connexin 43) in sorted epididymal EGFP$^+$ MPs from CX3CR1$^{EGFP/+}$ HET and CX3CR1$^{EGFP/EGFP}$ KO mice. (i) FACS strategy used to sort EGFP$^+$ cells from epididymides of HET and KO mice. (ii) Expression of *Gja1* gene (connexin 43) relative to the housekeeping gene *Gapdh*. EGFP$^+$ KO MPs showed a reduced expression of the *Gja1* gene compared to EGFP$^+$ HET MPs. Each dot represents EGFP$^+$-sorted cells from a pool of 2 epididymides from each mouse. Data were analyzed using Student's t-test. Data are shown as means ± SEM. **b** 3D confocal microscopy images showing EGFP$^+$ MPs (green) in close interaction with CD103$^+$ cells (pink) in the epididymides of CX3CR1$^{EGFP/+}$ HET and CX3CR1$^{EGFP/EGFP}$ KO mice. In the HET epididymis (panel *i*), CX3CR1$^+$ MPs and CD103$^+$ cells interact through the GJ protein connexin 43 (Cx43; red; arrow) (See also 3D reconstruction image in Video 3 for upper panel b*i*; Video 4 for lower panel b*i*). However, in the KO epididymis (panel *ii*) no apparent connexin 43 staining was detected at the cell–cell interaction site (See also 3D reconstruction image at Video 5 for upper panel b*ii*; Video 6 for lower panel b*ii*). Each image displays different cells. The site of interaction is highlighted by dashed white squares. Single Z-stack planes of the sites of interaction are shown in Suppl. Figure 7. Note that Cx43 (red dots) is also localized at the cell–cell interface between other cells. Nuclei are labeled with DAPI (blue). Bars: 5 µm

DCs. We revealed that epididymal CX3CR1$^+$ MP luminal-reaching dendrites can sense bacterial antigens and, therefore, severely reduce their membrane extrusions like what was reported after efferent duct ligation and vasectomy [13, 68]. These results reveal that the CX3CR1 receptor plays a key role in the immune response against bacterial antigens in the epididymis.

Our findings also show that the lack of CX3CR1 in the epididymis might confer protection upon the LPS challenge, indicating that CX3CR1 is involved in the pathophysiology

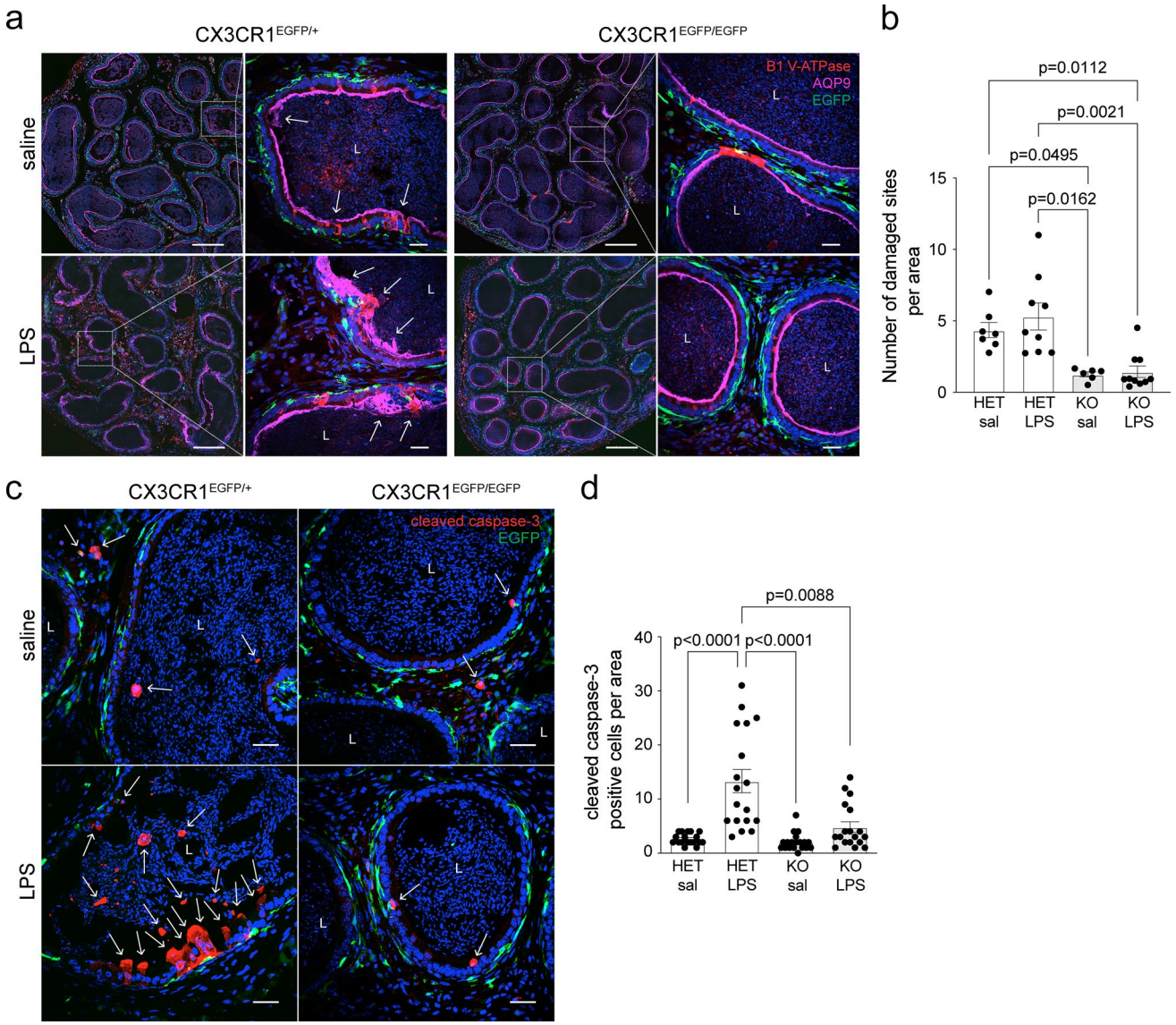

Fig. 7 Effect of the lack of CX3CR1 on epididymal epithelial cells after saline or LPS injections. **a** Confocal microscopy images showing immunolabeling of V-ATPase B1 subunit (red), a marker of clear cells, and AQP9 (pink), a marker of principal cells, in the cauda epididymis of CX3CR1$^{EGFP/+}$ HET and CX3CR1$^{EGFP/EGFP}$ KO mice 48 h after saline or LPS injection. The right panels show higher magnifications of the regions delineated by the white boxes in the left panels. EGFP^{+} MPs are displayed in green, and nuclei are labeled with DAPI (blue). Bars (left panels): 200 µm, Bars (right panels; magnifications): 20 µm. *L* lumen. **b** Quantification of the number of damaged sites normalized per area of tissue (µm^2) in the cauda of CX3CR1$^{EGFP/+}$ HET and CX3CR1$^{EGFP/EGFP}$ KO mice. Any morphological alteration in epididymal epithelia (arrows in **a**) was counted as a damaged site. In the HET epididymides, despite epididymal damage (arrows in **a**) being observed either after saline or LPS injections, injury was more severe in the LPS-treated group. Conversely, neither saline nor LPS injections damaged the epithelium in the cauda segments in the KO epididymides. Each area quantified is represented as a dot. **c** Cauda epididymis sections from HET and KO mice 48 h after saline or LPS-treatment were labeled for cleaved caspase-3 (red; arrows), an apoptotic marker. EGFP^{+} MPs are displayed in green, and nuclei are labeled with DAPI (blue). Bars: 20 µm. *L* lumen. **d** Quantification of the number of cleaved caspase-3 positive cells (apoptotic cells) in cauda of CX3CR1$^{EGFP/+}$ HET and CX3CR1$^{EGFP/EGFP}$ KO mice per area of tissue (39,600 µm^2). Deletion of CX3CR1 in MPs significantly reduced the number of apoptotic cells 48 h post-LPS compared to control (HET LPS). In the KO groups, no increase in the number of apoptotic cells per area was observed post-LPS compared to saline injection. Each image quantification is represented as a dot. Data were analyzed using the non-parametric Kruskal–Wallis test followed by Dunn's post hoc test. Data are shown as means ± SEM

of epididymitis. CX3CR1-deficient MPs might provide epididymal epithelial protection following infection by allowing repair mechanisms to occur and/or by attenuating further damage via reduction of inflammation. The latter mechanism is reinforced by the reduced numbers of apoptotic cells that we detected after LPS injection in the

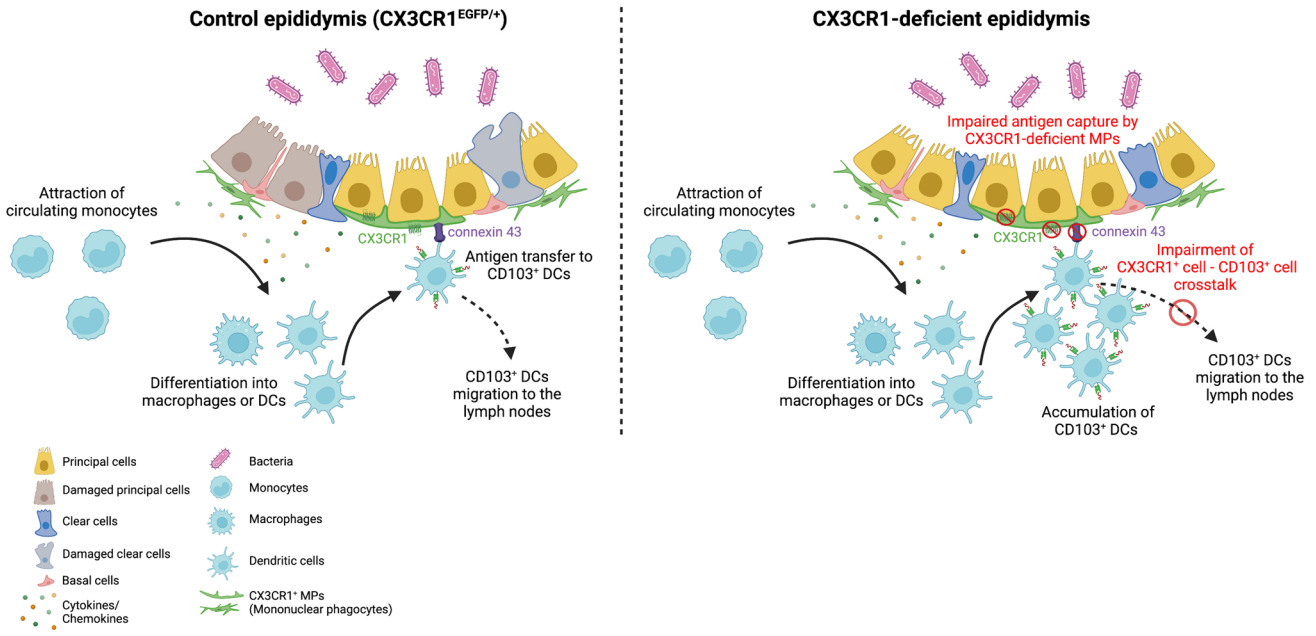

Fig. 8 Graphic scheme of the proposed CX3CR1^{+} MP-to-CD103^{+} DC crosstalk during bacterial antigen-induced epididymitis. Upon infection, in a control epididymis (left panel), cytokines and chemokines are released by epithelial cells, which attract circulating monocytes into the tissue. These attracted monocytes differentiate into macrophages and dendritic cells (DCs). CX3CR1^{+} MPs capture antigens and potentially transfer them to CD103^{+} DCs via the gap junction protein connexin 43. Consequently, CD103^{+} DCs migrate into the lymph nodes to start an immune response. In the absence of the CX3CR1 (right panel), there is infiltration of monocytes in the epididymis upon infection, which would then differentiate into macrophages or DCs. However, CX3CR1-deficient (KO) MPs display a potentially impaired cell-to-cell crosstalk between EGFP^{+} MPs and CD103^{+} DCs due to the downregulation of connexin 43 in the KO MPs. Consequently, these DCs would not migrate, and they would be accumulated in the interstitium of the organ. The lack of CX3CR1 modifies epididymal immune response followed by infection, which, in turn, could blunt the release of inflammatory molecules, resulting in less damage in the CX3CR1$^{EGFP/EGFP}$ KO epididymis. In addition, there is the possibility that EGFP^{+} KO MPs might also present a defective cell-to-cell crosstalk with epithelial cells, which might result in an inefficient MP-mediated response against infection. The figure was created with BioRender.com

CX3CR1$^{EGFP/EGFP}$ KO compared to the CX3CR1$^{EGFP/+}$ HET epididymides. Supporting this finding, the loss of CX3CR1 receptor or fractalkine chemokine was similarly shown to be protective in models of brain damage [69, 70] and acute renal injury [71]. Moreover, it is possible that CD103^{+} DCs, which are accumulated in the CX3CR1$^{EGFP/EGFP}$ KO epididymides after the LPS challenge, ameliorated LPS-induced epididymal damage as well. Indeed, in vivo CD103^{+} DC infusion alleviates liver injury [72]. EGFP^{+} KO MPs might also display impaired cell–cell communication with epithelial cells, resulting in a less efficient MP-mediated response against infection. However, we cannot rule out the possibility that, at a late time point, the infection could run uncontrolled in the KO epididymis, ultimately resulting in a more severely damaged epithelium. Additional studies will be required to elucidate the complex cell–cell communication networks of the MPs and epithelial cells in the epididymis. Together, our results indicate that the CX3CR1 signaling pathway might be a putative therapeutic target to disrupt the cascade of deleterious events that lead to injury.

In conclusion, our study provides evidence that the CX3CR1 receptor maintains tissue homeostasis by inducing luminal protrusion of MPs and by regulating the monocyte population in the epididymis at a steady state as well as following bacterial antigen exposure. In addition, we uncover the interaction between MPs and CD103^{+} dendritic cells, presumably through connexin 43, which may enhance immune responses during epididymitis. This interaction might be disrupted because of the downregulation of connexin 43 expression in CX3CR1$^{EGFP/EGFP}$ KO MPs. By providing a deeper understanding of the role of MPs in immune surveillance during sperm maturation and storage in the male excurrent duct, our study may lead to new and targeted therapies for common disorders such as male infertility and epididymitis, and identify potential targets for immuno-contraception.

Supplementary Information The online version contains supplementary material available at https://doi.org/10.1007/s00018-022-04664-w.

Acknowledgements The authors thank the Microscopy Core of the Program in Membrane Biology (PMB) (MGH, Boston, MA) and the

MGB Molecular Imaging Core (MGH, Charlestown, MA), in particular to Anil V. Nair and Mohammed Sami Saleh Mahamdeh, respectively, for their expertise and support in confocal microscopy. We also thank the HSCI-CRM Flow Cytometry Facility (MGH, Boston, MA), in particular Maris Handley, Daire D. Daly, and Jamie Kauffman for their guidance and assistance in flow cytometry analysis, and Yoshiko Iwamoto (Center for Systems Biology, Department of Radiology, MGH and Harvard Medical School, Boston, MA) for her help in performing the Hematoxylin and Eosin staining. We acknowledge Dr. Claudio Attardo-Parrinello for his assistance in performing one LPS experiment and Dr. Raul German Spallanzani for his assistance in the data interpretation.

Author contributions FB and MAB were involved in the study design and conceptualization. FB, KO, LJT, and MAB performed the experiments and data analysis. FB, RJS, DB, SB, and MAB were involved in data interpretation. FB and MAB wrote the original manuscript. All authors contributed to the writing of the manuscript, made critical comments, and approved the final version.

Funding This work was supported by the National Institutes of Health (grant HD104672-01 to M.A.B., grants HD040793, HD069623 to S.B.), the Lalor Foundation (to F.B.), and the IBSA Foundation for Scientific Research (to F.B.) The Microscopy Core facility of the Massachusetts General Hospital (MGH) Program in Membrane Biology receives support from the Boston Area Diabetes and Endocrinology Research Center (DK57521) and the Center for the Study of Inflammatory Bowel Disease (DK43351). The Zeiss LSM 800 microscope was acquired using an NIH Shared Instrumentation Grant S10-OD-021577–01. M.A.B is the recipient of the 2021 MGH Claflin Distinguished Scholar Research Award.

Data availability The datasets generated during this study are available from the corresponding author on reasonable request.

Declarations

Conflict of interest The authors have no relevant financial or non-financial interests to disclose.

Ethics approval All animal procedures were approved by the Massachusetts General Hospital (MGH) Subcommittee on Research Animal Care and were performed following the NIH Guide for the Care and Use of Laboratory Animals (National Academies Press, 2011; protocol 2003N000216).

References

1. Battistone MA, Mendelsohn AC, Spallanzani RG, Brown D, Nair AV, Breton S (2020) Region-specific transcriptomic and functional signatures of mononuclear phagocytes in the epididymis. Mol Hum Reprod 26(1):14–29. https://doi.org/10.1093/molehr/gaz059
2. Mendelsohn AC, Sanmarco LM, Spallanzani RG, Brown D, Quintana FJ, Breton S et al (2020) From initial segment to cauda: a regional characterization of mouse epididymal CD11c(+) mononuclear phagocytes based on immune phenotype and function. Am J Physiol Cell Physiol 319(6):C997–C1010. https://doi.org/10.1152/ajpcell.00392.2020
3. Wang M, Yang Y, Cansever D, Wang Y, Kantores C, Messiaen S et al (2021) Two populations of self-maintaining monocyte-independent macrophages exist in adult epididymis and testis. Proc Natl Acad Sci USA 118:1. https://doi.org/10.1073/pnas.2013686117
4. Da Silva N, Cortez-Retamozo V, Reinecker HC, Wildgruber M, Hill E, Brown D et al (2011) A dense network of dendritic cells populates the murine epididymis. Reproduction 141(5):653–663. https://doi.org/10.1530/REP-10-0493
5. Da Silva N, Smith TB (2015) Exploring the role of mononuclear phagocytes in the epididymis. Asian J Androl 17(4):591–596. https://doi.org/10.4103/1008-682X.153540
6. Hume DA (2006) The mononuclear phagocyte system. Curr Opin Immunol 18(1):49–53. https://doi.org/10.1016/j.coi.2005.11.008
7. Hume DA (2008) Differentiation and heterogeneity in the mononuclear phagocyte system. Mucosal Immunol 1(6):432–441. https://doi.org/10.1038/mi.2008.36
8. Gordon S, Pluddemann A (2019) The mononuclear phagocytic system generation of diversity. Front Immunol 10:1893. https://doi.org/10.3389/fimmu.2019.01893
9. Joeris T, Muller-Luda K, Agace WW, Mowat AM (2017) Diversity and functions of intestinal mononuclear phagocytes. Mucosal Immunol 10(4):845–864. https://doi.org/10.1038/mi.2017.22
10. Jakubzick CV, Randolph GJ, Henson PM (2017) Monocyte differentiation and antigen-presenting functions. Nat Rev Immunol 17(6):349–362. https://doi.org/10.1038/nri.2017.28
11. Holt PG, Haining S, Nelson DJ, Sedgwick JD (1994) Origin and steady-state turnover of class II MHC-bearing dendritic cells in the epithelium of the conducting airways. J Immunol 153(1):256–61. https://www.ncbi.nlm.nih.gov/pubmed/8207240
12. Voisin A, Whitfield M, Damon-Soubeyrand C, Goubely C, Henry-Berger J, Saez F et al (2018) Comprehensive overview of murine epididymal mononuclear phagocytes and lymphocytes: unexpected populations arise. J Reprod Immunol 126:11–17. https://doi.org/10.1016/j.jri.2018.01.003
13. Smith TB, Cortez-Retamozo V, Grigoryeva LS, Hill E, Pittet MJ, Da Silva N (2014) Mononuclear phagocytes rapidly clear apoptotic epithelial cells in the proximal epididymis. Andrology 2(5):755–762. https://doi.org/10.1111/j.2047-2927.2014.00251.x
14. Battistone MA, Spallanzani RG, Mendelsohn AC, Capen D, Nair AV, Brown D et al (2019) Novel role of proton-secreting epithelial cells in sperm maturation and mucosal immunity. J Cell Sci 133:5. https://doi.org/10.1242/jcs.233239
15. Silva EJR, Ribeiro CM, Mirim AFM, Silva AAS, Romano RM, Hallak J et al (2018) Lipopolysaccharide and lipotheicoic acid differentially modulate epididymal cytokine and chemokine profiles and sperm parameters in experimental acute epididymitis. Sci Rep 8(1):103. https://doi.org/10.1038/s41598-017-17944-4
16. Wang F, Liu W, Jiang Q, Gong M, Chen R, Wu H et al (2019) Lipopolysaccharide-induced testicular dysfunction and epididymitis in mice: a critical role of tumor necrosis factor alpha. Biol Reprod 100(3):849–861. https://doi.org/10.1093/biolre/ioy235
17. McLachlan RI (2002) Basis, diagnosis and treatment of immunological infertility in men. J Reprod Immunol 57(1–2):35–45. https://doi.org/10.1016/s0165-0378(02)00014-1
18. Meinhardt A, Hedger MP (2011) Immunological, paracrine and endocrine aspects of testicular immune privilege. Mol Cell Endocrinol 335(1):60–68. https://doi.org/10.1016/j.mce.2010.03.022
19. Busacca M, Fusi F, Brigante C, Doldi N, Smid M, Vigano P (1989) Evaluation of antisperm antibodies in infertile couples with immunobead test: prevalence and prognostic value. Acta Eur Fertil 20(2):77–82. https://www.ncbi.nlm.nih.gov/pubmed/2800931
20. Ferrer MS, Laflin S, Anderson DE, Miesner MD, Wilkerson MJ, George A et al (2015) Prevalence of bovine sperm-bound antisperm antibodies and their association with semen quality. Theriogenology 84(1):94–100. https://doi.org/10.1016/j.theriogenology.2015.02.017

21. Pierucci-Alves F, Midura-Kiela MT, Fleming SD, Schultz BD, Kiela PR (2018) Transforming growth factor beta signaling in dendritic cells is required for immunotolerance to sperm in the epididymis. Front Immunol 9:1882. https://doi.org/10.3389/fimmu.2018.01882
22. Warren BD, Ahn SH, Brittain KS, Nanjappa MK, Wang H, Wang J et al (2021) Multiple lesions contribute to infertility in males lacking autoimmune regulator. Am J Pathol 191(9):1592–1609. https://doi.org/10.1016/j.ajpath.2021.05.021
23. Fijak M, Pilatz A, Hedger MP, Nicolas N, Bhushan S, Michel V et al (2018) Infectious, inflammatory and "autoimmune" male factor infertility: how do rodent models inform clinical practice? Hum Reprod Update 24(4):416–441. https://doi.org/10.1093/humupd/dmy009
24. Klein B, Bhushan S, Gunther S, Middendorff R, Loveland KL, Hedger MP et al (2020) Differential tissue-specific damage caused by bacterial epididymo-orchitis in the mouse. Mol Hum Reprod 26(4):215–227. https://doi.org/10.1093/molehr/gaaa011
25. Pleuger C, Silva EJR, Pilatz A, Bhushan S, Meinhardt A (2020) Differential immune response to infection and acute inflammation along the epididymis. Front Immunol 11:599594. https://doi.org/10.3389/fimmu.2020.599594
26. Wijayarathna R, Pasalic A, Nicolas N, Biniwale S, Ravinthiran R, Genovese R et al (2020) Region-specific immune responses to autoimmune epididymitis in the murine reproductive tract. Cell Tissue Res 381(2):351–360. https://doi.org/10.1007/s00441-020-03215-8
27. Michel V, Pilatz A, Hedger MP, Meinhardt A (2015) Epididymitis: revelations at the convergence of clinical and basic sciences. Asian J Androl 17(5):756–763. https://doi.org/10.4103/1008-682X.155770
28. Rupp TJ, Leslie SW. Epididymitis. StatPearls, https://www.ncbi.nlm.nih.gov/pubmed/28613565. Treasure Island (FL)2022.
29. Banyra O, Shulyak A (2012) Acute epididymo-orchitis: staging and treatment. Cent Eur J Urol 65(3):139–143. https://doi.org/10.5173/ceju.2012.03.art8
30. Lai Y, Yu Z, Shi B, Ni L, Liu Y, Yang S (2014) Chronic scrotal pain caused by mild epididymitis: report of a series of 44 cases. Pak J Med Sci. 30(3):638–641. https://doi.org/10.12669/pjms.303.4256
31. Pilatz A, Hossain H, Kaiser R, Mankertz A, Schuttler CG, Domann E et al (2015) Acute epididymitis revisited: impact of molecular diagnostics on etiology and contemporary guideline recommendations. Eur Urol 68(3):428–435. https://doi.org/10.1016/j.eururo.2014.12.005
32. Michel V, Duan Y, Stoschek E, Bhushan S, Middendorff R, Young JM et al (2016) Uropathogenic *Escherichia coli* causes fibrotic remodelling of the epididymis. J Pathol 240(1):15–24. https://doi.org/10.1002/path.4748
33. Pleuger C, Ai D, Hoppe ML, Winter LT, Bohnert D, Karl D, et al (2022) The regional distribution of resident immune cells shapes distinct immunological environments along the murine epididymis. eLife 11:e82193. https://doi.org/10.7554/eLife.82193
34. Segel GB, Halterman MW, Lichtman MA (2011) The paradox of the neutrophil's role in tissue injury. J Leukoc Biol 89(3):359–372. https://doi.org/10.1189/jlb.0910538
35. Kruger P, Saffarzadeh M, Weber AN, Rieber N, Radsak M, von Bernuth H et al (2015) Neutrophils: between host defence, immune modulation, and tissue injury. PLoS Pathog 11(3):e1004651. https://doi.org/10.1371/journal.ppat.1004651
36. Breton S, Nair AV, Battistone MA (2019) Epithelial dynamics in the epididymis: role in the maturation, protection, and storage of spermatozoa. Andrology 7(5):631–643. https://doi.org/10.1111/andr.12632
37. Jung S, Aliberti J, Graemmel P, Sunshine MJ, Kreutzberg GW, Sher A et al (2000) Analysis of fractalkine receptor CX(3)CR1 function by targeted deletion and green fluorescent protein reporter gene insertion. Mol Cell Biol 20(11):4106–4114. https://doi.org/10.1128/MCB.20.11.4106-4114.2000
38. Battistone MA, Nair AV, Barton CR, Liberman RN, Peralta MA, Capen DE et al (2018) Extracellular adenosine stimulates vacuolar ATPase-dependent proton secretion in medullary intercalated cells. J Am Soc Nephrol 29(2):545–556. https://doi.org/10.1681/ASN.2017060643
39. Andrade AD, Almeida PGC, Mariani NAP, Freitas GA, Kushima H, Filadelpho AL et al (2021) Lipopolysaccharide-induced epididymitis modifies the transcriptional profile of Wfdc genes in mice. Biol Reprod 104(1):144–158. https://doi.org/10.1093/biolre/ioaa189
40. Barrachina F, Battistone MA, Castillo J, Mallofre C, Jodar M, Breton S et al (2022) Sperm acquire epididymis-derived proteins through epididymosomes. Hum Reprod 37(4):651–668. https://doi.org/10.1093/humrep/deac015
41. Brown D, Lydon J, McLaughlin M, Stuart-Tilley A, Tyszkowski R, Alper S (1996) Antigen retrieval in cryostat tissue sections and cultured cells by treatment with sodium dodecyl sulfate (SDS). Histochem Cell Biol 105(4):261–267. https://doi.org/10.1007/BF01463929
42. Kim B, Breton S (2022) The MAPK/ERK signaling pathway regulates the expression and localization of Cx43 in mouse proximal epididymis. Biol Reprod 106(5):919–927. https://doi.org/10.1093/biolre/ioac034
43. Pastor-Soler N, Bagnis C, Sabolic I, Tyszkowski R, McKee M, Van Hoek A et al (2001) Aquaporin 9 expression along the male reproductive tract. Biol Reprod 65(2):384–393. https://doi.org/10.1095/biolreprod65.2.384
44. Paunescu TG, Ljubojevic M, Russo LM, Winter C, McLaughlin MM, Wagner CA et al (2010) cAMP stimulates apical V-ATPase accumulation, microvillar elongation, and proton extrusion in kidney collecting duct A-intercalated cells. Am J Physiol Renal Physiol 298(3):F643–F654. https://doi.org/10.1152/ajprenal.00584.2009
45. Hulspas R, O'Gorman MR, Wood BL, Gratama JW, Sutherland DR (2009) Considerations for the control of background fluorescence in clinical flow cytometry. Cytometry B Clin Cytom 76(6):355–364. https://doi.org/10.1002/cyto.b.20485
46. Farache J, Koren I, Milo I, Gurevich I, Kim KW, Zigmond E et al (2013) Luminal bacteria recruit CD103+ dendritic cells into the intestinal epithelium to sample bacterial antigens for presentation. Immunity 38(3):581–595. https://doi.org/10.1016/j.immuni.2013.01.009
47. Mazzini E, Massimiliano L, Penna G, Rescigno M (2014) Oral tolerance can be established via gap junction transfer of fed antigens from CX3CR1(+) macrophages to CD103(+) dendritic cells. Immunity 40(2):248–261. https://doi.org/10.1016/j.immuni.2013.12.012
48. Coombes JL, Siddiqui KR, Arancibia-Carcamo CV, Hall J, Sun CM, Belkaid Y et al (2007) A functionally specialized population of mucosal CD103+ DCs induces Foxp3+ regulatory T cells via a TGF-beta and retinoic acid-dependent mechanism. J Exp Med 204(8):1757–1764. https://doi.org/10.1084/jem.20070590
49. Mese G, Richard G, White TW (2007) Gap junctions: basic structure and function. J Invest Dermatol 127(11):2516–2524. https://doi.org/10.1038/sj.jid.5700770
50. Barbe MT, Monyer H, Bruzzone R (2006) Cell-cell communication beyond connexins: the pannexin channels. Physiology (Bethesda) 21:103–114. https://doi.org/10.1152/physiol.00048.2005
51. Randolph GJ, Inaba K, Robbiani DF, Steinman RM, Muller WA (1999) Differentiation of phagocytic monocytes into lymph node

dendritic cells in vivo. Immunity 11(6):753–761. https://doi.org/10.1016/s1074-7613(00)80149-1
52. Jakubzick C, Tacke F, Ginhoux F, Wagers AJ, van Rooijen N, Mack M et al (2008) Blood monocyte subsets differentially give rise to CD103+ and CD103- pulmonary dendritic cell populations. J Immunol 180(5):3019–3027. https://doi.org/10.4049/jimmunol.180.5.3019
53. Varol C, Landsman L, Fogg DK, Greenshtein L, Gildor B, Margalit R et al (2007) Monocytes give rise to mucosal, but not splenic, conventional dendritic cells. J Exp Med 204(1):171–180. https://doi.org/10.1084/jem.20061011
54. Vermaelen KY, Carro-Muino I, Lambrecht BN, Pauwels RA (2001) Specific migratory dendritic cells rapidly transport antigen from the airways to the thoracic lymph nodes. J Exp Med 193(1):51–60. https://doi.org/10.1084/jem.193.1.51
55. Bedoui S, Whitney PG, Waithman J, Eidsmo L, Wakim L, Caminschi I et al (2009) Cross-presentation of viral and self antigens by skin-derived CD103+ dendritic cells. Nat Immunol 10(5):488–495. https://doi.org/10.1038/ni.1724
56. Helft J, Ginhoux F, Bogunovic M, Merad M (2010) Origin and functional heterogeneity of non-lymphoid tissue dendritic cells in mice. Immunol Rev 234(1):55–75. https://doi.org/10.1111/j.0105-2896.2009.00885.x
57. Chieppa M, Rescigno M, Huang AY, Germain RN (2006) Dynamic imaging of dendritic cell extension into the small bowel lumen in response to epithelial cell TLR engagement. J Exp Med 203(13):2841–2852. https://doi.org/10.1084/jem.20061884
58. Niess JH, Brand S, Gu X, Landsman L, Jung S, McCormick BA et al (2005) CX3CR1-mediated dendritic cell access to the intestinal lumen and bacterial clearance. Science 307(5707):254–258. https://doi.org/10.1126/science.1102901
59. Morita N, Umemoto E, Fujita S, Hayashi A, Kikuta J, Kimura I et al (2019) GPR31-dependent dendrite protrusion of intestinal CX3CR1(+) cells by bacterial metabolites. Nature 566(7742):110–114. https://doi.org/10.1038/s41586-019-0884-1
60. Reshef R, Kudryavitskaya E, Shani-Narkiss H, Isaacson B, Rimmerman N, Mizrahi A et al (2017) The role of microglia and their CX3CR1 signaling in adult neurogenesis in the olfactory bulb. Elife. https://doi.org/10.7554/eLife.30809
61. Cardona SM, Kim SV, Church KA, Torres VO, Cleary IA, Mendiola AS et al (2018) Role of the fractalkine receptor in CNS autoimmune inflammation: new approach utilizing a mouse model expressing the human CX3CR1(I249/M280) variant. Front Cell Neurosci 12:365. https://doi.org/10.3389/fncel.2018.00365
62. Geissmann F, Jung S, Littman DR (2003) Blood monocytes consist of two principal subsets with distinct migratory properties. Immunity 19(1):71–82. https://doi.org/10.1016/s1074-7613(03)00174-2
63. Browne JA, Yang R, Leir SH, Eggener SE, Harris A (2016) Expression profiles of human epididymis epithelial cells reveal the functional diversity of caput, corpus and cauda regions. Mol Hum Reprod 22(2):69–82. https://doi.org/10.1093/molehr/gav066
64. Rinaldi VD, Donnard E, Gellatly K, Rasmussen M, Kucukural A, Yukselen O et al (2020) An atlas of cell types in the mouse epididymis and vas deferens. Elife. https://doi.org/10.7554/eLife.55474
65. Liu P, Yu YR, Spencer JA, Johnson AE, Vallanat CT, Fong AM et al (2008) CX3CR1 deficiency impairs dendritic cell accumulation in arterial intima and reduces atherosclerotic burden. Arterioscler Thromb Vasc Biol 28(2):243–250. https://doi.org/10.1161/ATVBAHA.107.158675
66. Hulsmans M, Clauss S, Xiao L, Aguirre AD, King KR, Hanley A et al (2017) Macrophages facilitate electrical conduction in the heart. Cell 169(3):510–522. https://doi.org/10.1016/j.cell.2017.03.050
67. Zhao H, Yu C, He C, Mei C, Liao A, Huang D (2020) The immune characteristics of the epididymis and the immune pathway of the epididymitis caused by different pathogens. Front Immunol 11:2115. https://doi.org/10.3389/fimmu.2020.02115
68. Mullen TE Jr, Kiessling RL, Kiessling AA (2003) Tissue-specific populations of leukocytes in semen-producing organs of the normal, hemicastrated, and vasectomized mouse. AIDS Res Hum Retroviruses 19(3):235–243. https://doi.org/10.1089/0889222037 63315740
69. Denes A, Ferenczi S, Halasz J, Kornyei Z, Kovacs KJ (2008) Role of CX3CR1 (fractalkine receptor) in brain damage and inflammation induced by focal cerebral ischemia in mouse. J Cereb Blood Flow Metab 28(10):1707–1721. https://doi.org/10.1038/jcbfm.2008.64
70. Soriano SG, Amaravadi LS, Wang YF, Zhou H, Yu GX, Tonra JR et al (2002) Mice deficient in fractalkine are less susceptible to cerebral ischemia-reperfusion injury. J Neuroimmunol 125(1–2):59–65. https://doi.org/10.1016/s0165-5728(02)00033-4
71. Oh DJ, Dursun B, He Z, Lu L, Hoke TS, Ljubanovic D et al (2008) Fractalkine receptor (CX3CR1) inhibition is protective against ischemic acute renal failure in mice. Am J Physiol Renal Physiol 294(1):F264–F271. https://doi.org/10.1152/ajprenal.00204.2007
72. Zhou CZ, Wang RF, Cheng DL, Zhu YJ, Cao Q, Lv WF (2019) FLT3/FLT3L-mediated CD103(+) dendritic cells alleviates hepatic ischemia-reperfusion injury in mice via activation of treg cells. Biomed Pharmacother 118:109031. https://doi.org/10.1016/j.biopha.2019.109031